Scaling Calculation of Isoscalar Giant Resonances in Relativistic Thomas–Fermi Theory

S.K. Patra[1], X. Viñas, M. Centelles and M. Del Estal

Departament d'Estructura i Constituents de la Matèria, Facultat de Física,

Universitat de Barcelona, Diagonal 647, E-08028 Barcelona, Spain

Abstract

We derive analytical expressions for the excitation energy of the isoscalar giant monopole and quadrupole resonances in finite nuclei, by using the scaling method and the extended Thomas–Fermi approach to relativistic mean field theory. We study the ability of several non-linear $\sigma - \omega$ parameter sets of common use in reproducing the experimental data. For monopole oscillations the calculations agree better with experiment when the nuclear matter incompressibility of the relativistic interaction lies in the range 220–260 MeV. The breathing-mode energies of the scaling method compare satisfactorily with those obtained in relativistic RPA and time-dependent mean field calculations. For quadrupole oscillations all the analyzed non-linear parameter sets reproduce the empirical trends reasonably well.

PACS: 24.30.Cz, 21.60.-n, 21.30.Fe, 21.65.+f

Keywords: Giant resonances, Relativistic mean field, Scaling, Semiclassical methods, Thomas–Fermi theory, Nuclear incompressibility

[1]Present address: *Institute of Physics, Sachivalaya Marg, Bhubaneswar-751 005, India*

1 Introduction

The relativistic mean field (RMF) approach to Quantum Hadrodynamics [1] has become a very useful tool for describing ground-state properties of nuclei along the periodic table. The simplest model, the linear $\sigma - \omega$ model of Walecka [2], describes the nuclear force in terms of the exchange of σ and ω mesons. It is known that the value of the nuclear matter incompressibility is unreasonably high in this linear model ($K_\infty \sim 550$ MeV), which is a serious drawback for a precise description of some properties of finite nuclei and of collective excitations such as the breathing mode (isoscalar giant monopole resonance). The problem can be cured by introducing cubic and quartic self-interactions of the σ meson [3], which in particular have the effect of lowering the incompressibility, and the model can be refined by adding an isovector ρ meson. Current non-linear parameter sets, such as the NL3 parametrization [4], give ground-state binding energies and densities in very good agreement with the experimental data, not only for magic nuclei but also for deformed nuclei as well as for nuclei far from the stability line.

The RMF model has also been applied to describe dynamical collective motions in nuclei. The basic theory of vibrational states in nuclei, the random-phase approximation (RPA) [5,6], has been generalized to the relativistic domain (RRPA) [7,8,9] and it has been used in calculations of isoscalar giant resonances, to obtain response functions and mean energies for several magic nuclei. Small-amplitude collective motions such as the isovector dipole oscillation and the isoscalar and isovector quadrupole oscillations [10], as well as the isoscalar and isovector monopole oscillations [11], have been studied in the time-dependent RMF approach. Another approach is based on constrained RMF calculations. It has been applied to obtain breathing-mode energies and incompressibilities in the linear [12,13] and non-linear [14,15] $\sigma - \omega$ models. The generator coordinate method, with generating functions that are solutions of constrained RMF calculations, has been employed to compute excitation energies and transition densities of giant monopole states [11,14]. Other calculations of breathing-mode energies in the relativistic framework, see Refs. [15,16,17], have relied on the scaling model in combination with the leptodermous expansion of the finite nucleus incompressibility derived by Blaizot [18].

In the non-relativistic framework it is well established that the RPA is the small amplitude limit of the time-dependent Hartree–Fock approach [6,19]. In the relativistic case the RPA configuration space must include negative energy states from the Dirac sea in order to reproduce the results of time-dependent RMF or constrained RMF calculations [9,20]. Paraphrasing the statement, the RRPA corresponds to the small amplitude limit of the time-dependent RMF theory in the no-sea approximation when the RRPA includes both positive energy particle-hole pairs, and pairs formed from the empty Dirac sea states and the occupied Fermi sea states.

Semiclassical methods in nuclear physics, like the Thomas–Fermi theory, have proven to be very helpful for dealing with nuclear properties of global character that vary smoothly with the particle number A (e.g., binding energies, densities and their moments) [6,21,22,23]. The success of these methods stems from the fact that the shell corrections (quantal effects) are small as compared to the smooth part given by the semiclassical calculation. Semiclassical techniques like nuclear fluid dynamics [24] and the extended Thomas–Fermi method [25,26,27] have been applied to study giant resonances in non-relativistic models. In the relativistic context, the nuclear fluid dynamics approach has been utilized, e.g., in Refs. [28,29,30]. The authors of Refs. [31,32] resorted to a local Lorentz boost and the scaling method to study isoscalar giant monopole and quadrupole states in the linear $\sigma - \omega$ model. The investigations were carried out for nuclear matter (where a Thomas–Fermi approximation is exact) [31] and for symmetric, uncharged finite nuclei [32] whose densities were solved in the relativistic Thomas–Fermi (RTF) approximation.

The relativistic extended Thomas–Fermi (RETF) method [33,34,35] is a refinement of the RTF method, which incorporates gradient corrections of order $\hbar^2$ to the pure RTF approximation. It was derived only a few years ago and it has since been applied in calculations of ground-state binding energies and radii of finite nuclei [34,36,37] and in investigations of nuclear surface properties [34,37,38,39]. In the present work we shall use the RTF and RETF approaches to calculate the excitation energies of the isoscalar giant monopole and quadrupole resonances in spherical nuclei. This will be done by means of the scaling method, within the framework of the non-linear $\sigma - \omega$ model and the RMF theory. We shall also

perform constrained calculations for the monopole state.

Recently, the basic theory derived in the RTF approach has been applied to discuss the virial theorem and to study the breathing-mode energy within the RMF theory [40]. In the present contribution we analyze our self-consistent method in depth. To our knowledge, for realistic non-linear parameter sets of the RMF theory, these are the first calculations of isoscalar giant resonances in finite nuclei carried out with the scaling method which are fully self-consistent (i.e., we do not make use of a leptodermous expansion as in previous scaling approaches [15,16,17]). Owing to the meson-exchange nature of the relativistic model one has to deal with finite range forces, which renders the scaling method more involved than, e.g., for non-relativistic zero-range Skyrme forces. Moreover, in contrast to the non-relativistic situation, there exist two different densities, namely the baryon and the scalar density, in accordance with the fact that one has two types of fields, the vector and the scalar field.

The article is organized as follows. After the introductory remarks, we collect the basic expressions of the energy density and the variational equations of the RTF and RETF models in Section 2. The third and fourth sections are devoted to the derivation of the equations and the discussion of the numerical applications for the giant monopole and quadrupole resonances, respectively. The conclusions are laid in the last section. Some technicalities and a derivation of the virial theorem for the relativistic model are given in the appendices.

2 Energy density and variational equations

The mean field Hartree energy density of a finite nucleus in the non-linear $\sigma - \omega$ model reads [1,2,3]

$$\mathcal{H} = \sum_i \varphi_i^\dagger \left[-i\boldsymbol{\alpha}\cdot\boldsymbol{\nabla} + \beta m^* + g_{\rm v} V + \frac{1}{2} g_\rho R \tau_3 + \frac{1}{2} e\mathcal{A}(1+\tau_3) \right] \varphi_i + \mathcal{H}_{\rm f}. \tag{2.1}$$

The relativistic effective mass (or Dirac mass) is defined by $m^* = m - g_{\rm s}\phi$, τ_3 is the third component of the isospin operator, and the subindex i runs over the occupied states φ_i of the positive energy spectrum. $\mathcal{H}_{\rm f}$ stands for the free contribution of the meson fields ϕ, V and R associated with the σ, ω and ρ mesons, respectively, and of the Coulomb field $\mathcal{A}$:

$$\begin{aligned} \mathcal{H}_{\rm f} &= \frac{1}{2}\left[(\boldsymbol{\nabla}\phi)^2 + m_{\rm s}^2\phi^2 \right] + \frac{1}{3} b\phi^3 + \frac{1}{4} c\phi^4 - \frac{1}{2}\left[(\boldsymbol{\nabla} V)^2 + m_{\rm v}^2 V^2 \right] \\ &\quad - \frac{1}{2}\left[(\boldsymbol{\nabla} R)^2 + m_\rho^2 R^2 \right] - \frac{1}{2}\left(\boldsymbol{\nabla}\mathcal{A} \right)^2 . \end{aligned} \tag{2.2}$$

It is understood that the densities and fields are local quantities that depend on position, even if we do not make it explicit in most of our expressions. Units are $\hbar = c = 1$.

The semiclassical representation of the energy density (2.1) has a similar structure, except that the nucleon variables are the neutron and proton densities ($\rho_{\rm n}$ and $\rho_{\rm p}$) instead of the wave functions. In the RETF approach it reads [34,36,37,38,39]

$$\mathcal{H} = \mathcal{E} + g_{\rm v} V \rho + g_\rho R \rho_3 + e\mathcal{A}\rho_{\rm p} + \mathcal{H}_{\rm f}, \tag{2.3}$$

where $\rho = \rho_{\rm p} + \rho_{\rm n}$ is the baryon density, $\rho_3 = \frac{1}{2}(\rho_{\rm p} - \rho_{\rm n})$ is the isovector density, and the nucleon energy density $\mathcal{E}$ is written as $\mathcal{E} = \mathcal{E}_0 + \mathcal{E}_2$ with

$$\mathcal{E}_0 = \sum_q \frac{1}{8\pi^2}\left[k_{{\rm F}q}\epsilon_{{\rm F}q}^3 + k_{{\rm F}q}^3 \epsilon_{{\rm F}q} - m^{*4} \ln \frac{k_{{\rm F}q} + \epsilon_{{\rm F}q}}{m^*} \right] \tag{2.4}$$

and

$$\mathcal{E}_2 = \sum_q \left[B_{1q}(k_{{\rm F}q}, m^*)(\boldsymbol{\nabla}\rho_q)^2 + B_{2q}(k_{{\rm F}q}, m^*)\left(\boldsymbol{\nabla}\rho_q \cdot \boldsymbol{\nabla} m^*\right) + B_{3q}(k_{{\rm F}q}, m^*)(\boldsymbol{\nabla} m^*)^2 \right]. \tag{2.5}$$

For each kind of nucleon ($q = {\rm n}, {\rm p}$), the local Fermi momentum $k_{{\rm F}q}$ and $\epsilon_{{\rm F}q}$ are defined by

$$k_{{\rm F}q} = (3\pi^2\rho_q)^{1/3}, \qquad \epsilon_{{\rm F}q} = \sqrt{k_{{\rm F}q}^2 + m^{*2}}. \tag{2.6}$$

The coefficients B_{iq} are the following functions of $k_{\mathrm{F}q}$ and m^* [34,39]:

$$\begin{aligned} B_{1q} &= \frac{\pi^2}{24k_{\mathrm{F}q}^3\epsilon_{\mathrm{F}q}^2}\left(\epsilon_{\mathrm{F}q}+2k_{\mathrm{F}q}\ln\frac{k_{\mathrm{F}q}+\epsilon_{\mathrm{F}q}}{m^*}\right), \\ B_{2q} &= \frac{m^*}{6k_{\mathrm{F}q}\epsilon_{\mathrm{F}q}^2}\ln\frac{k_{\mathrm{F}q}+\epsilon_{\mathrm{F}q}}{m^*}, \\ B_{3q} &= \frac{k_{\mathrm{F}q}^2}{24\pi^2\epsilon_{\mathrm{F}q}^2}\left[\frac{\epsilon_{\mathrm{F}q}}{k_{\mathrm{F}q}}-\left(2+\frac{\epsilon_{\mathrm{F}q}^2}{k_{\mathrm{F}q}^2}\right)\ln\frac{k_{\mathrm{F}q}+\epsilon_{\mathrm{F}q}}{m^*}\right]. \end{aligned} \tag{2.7}$$

The RTF approximation is obtained by neglecting $\mathcal{E}_2$ in Eq. (2.3). The gradients contained in $\mathcal{E}_2$ arise from the RETF corrections of order $\hbar^2$ to the functional $\mathcal{E}_0$. Naturally, these corrections are more important in the nuclear surface region where the densities and the fields change more rapidly.

The semiclassical ground-state densities and meson fields are obtained by solving the Euler–Lagrange equations $\delta\mathcal{H}/\delta\rho_q=\mu_q$ (with μ_q being the chemical potential) coupled to the field equations

$$(\Delta-m_{\mathrm{s}}^2)\phi = -g_{\mathrm{s}}\rho_{\mathrm{s}}+b\phi^2+c\phi^3, \tag{2.8}$$

$$(\Delta-m_{\mathrm{v}}^2)V = -g_{\mathrm{v}}\rho, \tag{2.9}$$

$$(\Delta-m_{\rho}^2)R = -g_{\rho}\rho_3, \tag{2.10}$$

$$\Delta\mathcal{A} = -e\rho_{\mathrm{p}}. \tag{2.11}$$

The semiclassical scalar density in (2.8) is given by

$$\begin{aligned} \rho_{\mathrm{s}} &= \frac{\delta\mathcal{E}_0}{\delta m^*}+\frac{\delta\mathcal{E}_2}{\delta m^*}=\rho_{\mathrm{s}0}+\rho_{\mathrm{s}2} \\ &= \sum_q\frac{m^*}{2\pi^2}\left[k_{\mathrm{F}q}\epsilon_{\mathrm{F}q}-m^{*2}\ln\frac{k_{\mathrm{F}q}+\epsilon_{\mathrm{F}q}}{m^*}\right] \\ &\quad -\sum_q\left[B_{2q}\Delta\rho_q+2B_{3q}\Delta m^*+\left(\frac{\partial B_{2q}}{\partial\rho_q}-\frac{\partial B_{1q}}{\partial m^*}\right)(\boldsymbol{\nabla}\rho_q)^2\right. \\ &\quad \left.+2\frac{\partial B_{3q}}{\partial\rho_q}(\boldsymbol{\nabla}\rho_q\cdot\boldsymbol{\nabla}m^*)+\frac{\partial B_{3q}}{\partial m^*}(\boldsymbol{\nabla}m^*)^2\right]. \end{aligned} \tag{2.12}$$

Parenthetically, we would like to mention that the densities ρ, $\rho_{\rm s}$ and $\mathcal{E}$ above are the semiclassical counterparts of the quantal densities $\rho = \sum_i \varphi_i^\dagger \varphi_i$, $\rho_{\rm s} = \sum_i \varphi_i^\dagger \beta \varphi_i$ and $\mathcal{E} = \sum_i \varphi_i^\dagger \left[-i\boldsymbol{\alpha}\cdot\boldsymbol{\nabla} + \beta m^*\right]\varphi_i$.

Since the energy density $\mathcal{H}$ is to be integrated over the space to compute the total energy, the field equations (2.8)–(2.11) can be used to rewrite $\mathcal{H}_{\rm f}$, e.g., by transforming $[(\boldsymbol{\nabla}V)^2 + m_{\rm v}^2 V^2]$ into $V(-\Delta + m_{\rm v}^2)V = g_{\rm v} V\rho$ (valid, of course, under an integral sign). This way, on defining an effective scalar density by

$$g_{\rm s}\rho_{\rm s}^{\rm eff} = g_{\rm s}\rho_{\rm s} - b\phi^2 - c\phi^3, \tag{2.13}$$

$\mathcal{H}$ can be recast as

$$\mathcal{H} = \mathcal{E} + \frac{1}{2}g_{\rm s}\phi\rho_{\rm s}^{\rm eff} + \frac{1}{3}b\phi^3 + \frac{1}{4}c\phi^4 + \frac{1}{2}g_{\rm v}V\rho + \frac{1}{2}g_\rho R\rho_3 + \frac{1}{2}e\mathcal{A}\rho_{\rm p}. \tag{2.14}$$

This form of $\mathcal{H}$ will be more convenient for facilitating the calculations to be presented below.

3 Giant monopole resonance

As far as the giant resonances are dynamical processes one must first describe the nucleus from a moving frame [31,32]. This is a rather technical matter for our present purposes and it is left for Appendix A, where we derive the expression of the energy of a nucleus within the relativistic model in a frame moving with velocity $-\boldsymbol{v}$. After performing the scaling of the energy in this frame, one obtains general expressions for the two main ingredients required for the calculation of the excitation energy of the giant resonance, namely, the restoring force and the mass or inertia parameter (Eqs. (A.12) and (A.13), respectively).

The present section proceeds as follows. We begin by introducing our scaling approach for the monopole vibration. Next we obtain analytical expressions for the restoring force and the mass parameter of the monopole state. The calculational details of the derivatives of the meson fields with respect to the collective coordinate of the monopole vibration are reserved for Appendix B, where we also discuss the virial theorem (stationarity of the scaled energy) for the relativistic model. Next in the section we give a brief summary of the constrained approach to the breathing mode, for comparison with the scaling approach. The section closes with the discussion of the results of our numerical calculations.

3.1 Scaling

Denoting by λ the collective coordinate associated with the monopole vibration, a normalized scaled version of the baryon density is

$$\rho_\lambda(\boldsymbol{r}) = \lambda^3 \rho(\lambda \boldsymbol{r}). \tag{3.1}$$

Accordingly, the local Fermi momentum changes as

$$k_{\mathrm{F}q\lambda}(\boldsymbol{r}) = [3\pi^2 \rho_{q\lambda}(\boldsymbol{r})]^{1/3} = \lambda k_{\mathrm{F}q}(\lambda \boldsymbol{r}). \tag{3.2}$$

The meson fields ϕ, V and R and the Coulomb field $\mathcal{A}$ are also modified by the scaling due to the self-consistent equations (2.8)–(2.11), which will relate the scaled fields to the scaled densities. Unfortunately, the meson fields do not scale according to simple laws like (3.1) and (3.2) because of the finite range of the meson interactions. This is most apparent for

the scalar field ϕ, since the scalar density in the source term of Eq. (2.8) transforms not only due to the scaling of $k_{\mathrm{F}q}$ but also of ϕ itself (or m^*), see Eq. (2.12) for ρ_{s}. For reasons that will become clear immediately, we shall write the scaled effective mass $m^*_\lambda(\boldsymbol{r}) = m - g_{\mathrm{s}}\phi_\lambda(\boldsymbol{r})$ in the form

$$m^*_\lambda(\boldsymbol{r}) \equiv \lambda \tilde{m}^*(\lambda \boldsymbol{r}). \tag{3.3}$$

Note that the quantity $\tilde{m}^*$ carries an implicit dependence on λ apart from the parametric dependence on $\lambda\boldsymbol{r}$.

On account of Eqs. (3.2) and (3.3) the scaled semiclassical energy density $\mathcal{E}_\lambda = \mathcal{E}_{0\lambda} + \mathcal{E}_{2\lambda}$ and scalar density $\rho_{\mathrm{s}\lambda} = \rho_{\mathrm{s}0\lambda} + \rho_{\mathrm{s}2\lambda}$ read

$$\mathcal{E}_\lambda(\boldsymbol{r}) = \lambda^4 \mathcal{E}_0[k_{\mathrm{F}q}(\lambda\boldsymbol{r}), \tilde{m}^*(\lambda\boldsymbol{r})] + \lambda^4 \mathcal{E}_2[k_{\mathrm{F}q}(\lambda\boldsymbol{r}), \tilde{m}^*(\lambda\boldsymbol{r})] \equiv \lambda^4 \tilde{\mathcal{E}}(\lambda\boldsymbol{r}), \tag{3.4}$$

$$\rho_{\mathrm{s}\lambda}(\boldsymbol{r}) = \lambda^3 \rho_{\mathrm{s}0}[k_{\mathrm{F}q}(\lambda\boldsymbol{r}), \tilde{m}^*(\lambda\boldsymbol{r})] + \lambda^3 \rho_{\mathrm{s}2}[k_{\mathrm{F}q}(\lambda\boldsymbol{r}), \tilde{m}^*(\lambda\boldsymbol{r})] \equiv \lambda^3 \tilde{\rho}_{\mathrm{s}}(\lambda\boldsymbol{r}). \tag{3.5}$$

The tilded quantities $\tilde{\mathcal{E}}$ and $\tilde{\rho}_{\mathrm{s}}$ are given by Eqs. (2.4), (2.5) and (2.12) after replacing m^* by $\tilde{m}^*$. Note the usefulness of (3.3) to be able to write (3.4) and (3.5) in this compact form. For the scaled total energy density $\mathcal{H}_\lambda$ we obtain

$$\mathcal{H}_\lambda = \lambda^3 \Big[\lambda \tilde{\mathcal{E}} + \frac{1}{2} g_{\mathrm{s}} \phi_\lambda \tilde{\rho}_{\mathrm{s}}^{\mathrm{eff}} + \frac{1}{3} \frac{b}{\lambda^3} \phi_\lambda^3 + \frac{1}{4} \frac{c}{\lambda^3} \phi_\lambda^4 + \frac{1}{2} g_{\mathrm{v}} V_\lambda \rho + \frac{1}{2} g_\rho R_\lambda \rho_3 + \frac{1}{2} e \mathcal{A}_\lambda \rho_{\mathrm{p}} \Big], \tag{3.6}$$

with the definition

$$g_{\mathrm{s}} \tilde{\rho}_{\mathrm{s}}^{\mathrm{eff}} = g_{\mathrm{s}} \tilde{\rho}_{\mathrm{s}} - \frac{b}{\lambda^3} \phi_\lambda^2 - \frac{c}{\lambda^3} \phi_\lambda^3. \tag{3.7}$$

Observe that the same expression is valid regardless of performing the calculations in the RETF model or in the RTF model, as the corrections of order $\hbar^2$ ($\mathcal{E}_2$ and $\rho_{\mathrm{s}2}$) scale in the same manner as the the Thomas–Fermi terms ($\mathcal{E}_0$ and $\rho_{\mathrm{s}0}$).

3.2 Restoring force

The restoring force C_{M} of the monopole vibration is given by the second derivative of the scaled energy with respect to the collective coordinate λ, calculated at $\lambda = 1$ (Appendix A). The first derivative of the scaled energy is

$$\frac{\partial}{\partial\lambda} \int d(\lambda\boldsymbol{r}) \frac{\mathcal{H}_\lambda(\boldsymbol{r})}{\lambda^3} = \int d(\lambda\boldsymbol{r}) \Big[\tilde{\mathcal{E}} - \tilde{m}^* \tilde{\rho}_{\mathrm{s}} - \frac{1}{2} g_{\mathrm{s}} \tilde{\rho}_{\mathrm{s}}^{\mathrm{eff}} \frac{\partial \phi_\lambda}{\partial \lambda} + \frac{1}{2} g_{\mathrm{s}} \phi_\lambda \frac{\partial \tilde{\rho}_{\mathrm{s}}^{\mathrm{eff}}}{\partial \lambda} - \frac{b}{\lambda^4} \phi_\lambda^3$$

$$- \frac{3}{4}\frac{c}{\lambda^4}\phi_\lambda^4 + \frac{1}{2}g_{\rm v}\rho\frac{\partial V_\lambda}{\partial\lambda} + \frac{1}{2}g_\rho\rho_3\frac{\partial R_\lambda}{\partial\lambda} + \frac{1}{2}e\rho_{\rm p}\frac{\partial\mathcal{A}_\lambda}{\partial\lambda}\Bigg]. \tag{3.8}$$

Here we have used $\partial\tilde{\mathcal{E}}/\partial\lambda = \tilde{\rho}_{\rm s}\,\partial\tilde{m}^*/\partial\lambda$ (as $\tilde{\rho}_{\rm s} = \delta\tilde{\mathcal{E}}/\delta\tilde{m}^*$) and

$$\frac{\partial m_\lambda^*}{\partial\lambda} = \tilde{m}^* + \lambda\frac{\partial\tilde{m}^*}{\partial\lambda} = -g_{\rm s}\frac{\partial\phi_\lambda}{\partial\lambda}, \tag{3.9}$$

from the definition (3.3) of $\tilde{m}^*$. Differentiating again with respect to λ and then setting $\lambda = 1$ we have

$$\begin{aligned} C_{\rm M} &= \left[\frac{\partial^2}{\partial\lambda^2}\int d(\lambda\boldsymbol{r})\frac{\mathcal{H}_\lambda(\boldsymbol{r})}{\lambda^3}\right]_{\lambda=1} = \\ &\int d\boldsymbol{r}\left[-\tilde{m}^*\frac{\partial\tilde{\rho}_{\rm s}}{\partial\lambda} - \frac{1}{2}g_{\rm s}\tilde{\rho}_{\rm s}^{\rm eff}\frac{\partial^2\phi_\lambda}{\partial\lambda^2} + \frac{1}{2}g_{\rm s}\phi_\lambda\frac{\partial^2\tilde{\rho}_{\rm s}^{\rm eff}}{\partial\lambda^2} + 4\frac{b}{\lambda^5}\phi_\lambda^3 + 3\frac{c}{\lambda^5}\phi_\lambda^4\right. \\ &\left. - \frac{3}{\lambda^4}(b\phi_\lambda^2 + c\phi_\lambda^3)\frac{\partial\phi_\lambda}{\partial\lambda} + \frac{1}{2}g_{\rm v}\rho\frac{\partial^2 V_\lambda}{\partial\lambda^2} + \frac{1}{2}g_\rho\rho_3\frac{\partial^2 R_\lambda}{\partial\lambda^2} + \frac{1}{2}e\rho_{\rm p}\frac{\partial^2\mathcal{A}_\lambda}{\partial\lambda^2}\right]_{\lambda=1}. \end{aligned} \tag{3.10}$$

The calculation of the derivatives of the scaled meson fields with respect to λ is illustrated in Appendix B. There we also work out Eq. (3.8) at $\lambda = 1$, which leads to the virial theorem (stationarity condition of the energy) for the relativistic mean field model. Following the technique outlined in Appendix B we find

$$\left.\frac{\partial^2 V_\lambda(\boldsymbol{r})}{\partial\lambda^2}\right|_{\lambda=1} = \int d\boldsymbol{r}'\rho(\boldsymbol{r}')\left[2s\frac{d\mathcal{V}_\omega(s)}{ds} + s^2\frac{d^2\mathcal{V}_\omega(s)}{ds^2}\right], \tag{3.11}$$

with

$$\mathcal{V}_\omega(s) = \frac{g_{\rm v}}{4\pi}\frac{e^{-m_{\rm v}s}}{s}, \qquad s = |\boldsymbol{r} - \boldsymbol{r}'|. \tag{3.12}$$

An equivalent expression holds for the field R_λ. As is well known, the second derivative of the scaled Coulomb field $\mathcal{A}_\lambda$ vanishes [19] (you only have to evaluate (3.11) for a zero meson mass). For the scalar field one gets a lengthier expression owing to the extra implicit dependence of $\tilde{\rho}_{\rm s}^{\rm eff}$ on λ:

$$\begin{aligned} \left.\frac{\partial^2\phi_\lambda(\boldsymbol{r})}{\partial\lambda^2}\right|_{\lambda=1} &= \int d\boldsymbol{r}'\rho_{\rm s}^{\rm eff}(\boldsymbol{r}')\left[2s\frac{d\mathcal{V}_\sigma(s)}{ds} + s^2\frac{d^2\mathcal{V}_\sigma(s)}{ds^2}\right] \\ &\quad - \int d\boldsymbol{r}'\left[2s\frac{d\mathcal{V}_\sigma(s)}{ds}\frac{\partial\tilde{\rho}_{\rm s}^{\rm eff}(\lambda\boldsymbol{r}')}{\partial\lambda} - \mathcal{V}_\sigma(s)\frac{\partial^2\tilde{\rho}_{\rm s}^{\rm eff}(\lambda\boldsymbol{r}')}{\partial\lambda^2}\right]_{\lambda=1}. \end{aligned} \tag{3.13}$$

Inserting these results into Eq. (3.10) for $C_{\rm M}$ we end up with

$$\begin{aligned} C_{\rm M} &= \int d\boldsymbol{r} \left\{ \left[-\tilde{m}^* \frac{\partial \tilde{\rho}_{\rm s}}{\partial \lambda} + g_{\rm s} \frac{\partial \tilde{\rho}_{\rm s}^{\rm eff}}{\partial \lambda} \int d\boldsymbol{r}' \rho_{\rm s}^{\rm eff}(\boldsymbol{r}') s \frac{d\mathcal{V}_\sigma}{ds} - 3(b\phi^2 + c\phi^3) \frac{\partial \phi_\lambda}{\partial \lambda} \right]_{\lambda=1} \right. \\ &\quad - \frac{1}{2} g_{\rm s} \rho_{\rm s}^{\rm eff} \int d\boldsymbol{r}' \rho_{\rm s}^{\rm eff}(\boldsymbol{r}') \left[2s \frac{d\mathcal{V}_\sigma}{ds} + s^2 \frac{d^2\mathcal{V}_\sigma}{ds^2} \right] + 4b\phi^3 + 3c\phi^4 \\ &\quad + \frac{1}{2} g_{\rm v} \rho \int d\boldsymbol{r}' \rho(\boldsymbol{r}') \left[2s \frac{d\mathcal{V}_\omega}{ds} + s^2 \frac{d^2\mathcal{V}_\omega}{ds^2} \right] \\ &\quad \left. + \frac{1}{2} g_\rho \rho_3 \int d\boldsymbol{r}' \rho_3(\boldsymbol{r}') \left[2s \frac{d\mathcal{V}_\rho}{ds} + s^2 \frac{d^2\mathcal{V}_\rho}{ds^2} \right] \right\}, \end{aligned} \tag{3.14}$$

After some algebra it is possible to recast the restoring force of the monopole state as

$$\begin{aligned} C_{\rm M} &= \int d\boldsymbol{r} \left[-m \frac{\partial \tilde{\rho}_{\rm s}}{\partial \lambda} + 3 \left(m_{\rm s}^2 \phi^2 + \frac{1}{3} b\phi^3 - m_{\rm v}^2 V^2 - m_\rho^2 R^2 \right) \right. \\ &\quad \left. - (2m_{\rm s}^2 \phi + b\phi^2) \frac{\partial \phi_\lambda}{\partial \lambda} + 2m_{\rm v}^2 V \frac{\partial V_\lambda}{\partial \lambda} + 2m_\rho^2 R \frac{\partial R_\lambda}{\partial \lambda} \right]_{\lambda=1}. \end{aligned} \tag{3.15}$$

Note that as in the case of $\mathcal{H}_\lambda$ the same expression holds in both the RTF and RETF models. In each model one just has to compute $C_{\rm M}$ with the ground-state densities and fields obtained from the solution of the corresponding variational equations (which are modified by the inclusion of the corrections $\mathcal{E}_2$ and $\rho_{\rm s2}$). The derivatives with respect to λ entering Eq. (3.15) can be calculated as indicated in Appendix B, Eqs. (B.4)–(B.7). We have found $C_{\rm M}$ to take positive values for all of the (linear and non-linear) parameter sets we have used in the RTF and RETF calculations. A large part of the final value of $C_{\rm M}$ (usually far more than a half) is due to the contribution of the term $-m\partial\tilde{\rho}_{\rm s}/\partial\lambda|_{\lambda=1}$.

Evaluation of the integrand of Eq. (3.15) in the limit of symmetric infinite nuclear matter gives the result

$$K_\infty \rho_\infty = 9 \frac{g_{\rm v}^2}{m_{\rm v}^2} \rho_\infty^2 + 3 \frac{k_{\rm F,\infty}^2}{\epsilon_{\rm F,\infty}} \rho_\infty + 3 \frac{m_\infty^*}{\epsilon_{\rm F,\infty}} \rho_\infty \left. \frac{\partial \tilde{m}_\infty^*}{\partial \lambda} \right|_{\lambda=1}. \tag{3.16}$$

From the field equation for the scaled scalar field in nuclear matter we have

$$\left. \frac{\partial \tilde{m}_\infty^*}{\partial \lambda} \right|_{\lambda=1} = -3 g_{\rm s}^2 \frac{m_\infty^*}{\epsilon_{\rm F,\infty}} \rho_\infty \left[m_{\rm s}^2 + 3 g_{\rm s}^2 \left(\frac{\rho_{\rm s,\infty}}{m_\infty^*} - \frac{\rho_\infty}{\epsilon_{\rm F,\infty}} \right) + 2b\phi_\infty^2 + 3c\phi_\infty^3 \right]^{-1}, \tag{3.17}$$

and, as expected, K_∞ in (3.16) is seen to coincide with the expression of the bulk nuclear incompressibility in the relativistic model [37,38].

3.3 Mass parameter

As explained in Appendix A the mass parameter of the giant resonance is obtained from the second derivative of the scaled energy in a moving frame with respect to the collective velocity $\dot{\lambda} = d\lambda/dt$, see Eq. (A.13). The relation between the collective velocity $\dot{\lambda}$ and the velocity $\boldsymbol{v}$ of the moving frame is provided by the continuity equation (A.15) for the scaled system. This equation suggests a radial velocity field of the form $\boldsymbol{v} = -\dot{\lambda}u(r)\boldsymbol{r}/r$ up to first order in $\dot{\lambda}$ for the monopole mode [12,13,15]. In terms of the displacement field $u(r)$ the mass parameter (A.13) is written as

$$B = \int d\boldsymbol{r} u^2(r)\mathcal{H}, \tag{3.18}$$

while the continuity equation (A.15) becomes

$$\frac{d\rho_\lambda(\boldsymbol{r})}{d\lambda} - \nabla \cdot \left[\rho_\lambda(\boldsymbol{r})u(r)\frac{\boldsymbol{r}}{r}\right] = 0. \tag{3.19}$$

At $\lambda = 1$ Eq. (3.19) determines the displacement field as

$$u(r) = \frac{1}{\rho(r)r^2}\int_0^r dr' r'^2 \rho_{\rm T}(r'), \tag{3.20}$$

where

$$\rho_{\rm T}(\boldsymbol{r}) = \left.\frac{d\rho_\lambda(\boldsymbol{r})}{d\lambda}\right|_{\lambda=1} \tag{3.21}$$

is the so-called transition density.

For the monopole mode $\rho_\lambda(\boldsymbol{r}) = \lambda^3\rho(\lambda\boldsymbol{r})$ and, thus, the transition density is given by

$$\rho_{\rm T}(r) = 3\rho(r) + r\frac{d\rho(r)}{dr}, \tag{3.22}$$

which is known as the Tassie transition density. Partial integration of Eq. (3.20) with (3.22) leads to the well-known result $u(r) = r$ for the displacement field under the scaling transformation. The mass parameter of the monopole oscillation thus becomes [31,32]

$$B_{\rm M} = \int d\boldsymbol{r} r^2 \mathcal{H}. \tag{3.23}$$

Finally one calculates the excitation energy of the monopole state in the scaling model as

$$\bar{E}^{\rm s}_{\rm M} = \sqrt{\frac{C_{\rm M}}{B_{\rm M}}}. \tag{3.24}$$

Let us mention in passing that in the non-relativistic approach the mass parameter is derived as $B_{\rm M}^{\rm nr} = \int d\boldsymbol{r} r^2 m\rho$, with m being the nucleon mass. Actually, provided that $B_{\rm M}$ is replaced by $B_{\rm M}^{\rm nr}$ in (3.24), the scaling energy of the monopole vibration can be formally expressed as in the non-relativistic sum-rule approach. That is, $\bar{E}_{\rm M}^{\rm s} = \sqrt{m_3/m_1}$, where the moment m_1 is the energy weighted sum rule

$$m_1 = \frac{2}{m} A\langle r^2\rangle = \frac{2}{m^2} B_{\rm M}^{\rm nr}, \tag{3.25}$$

and m_3 is the plus three energy moment related to the second derivative of the scaled energy [19].

3.4 Constrained calculation

The giant monopole resonance can also be studied by performing a constrained calculation. In the semiclassical context one has to minimize the constrained functional

$$\int d\boldsymbol{r}[\mathcal{H} - \eta r^2\rho] = E(\eta) - \eta \int d\boldsymbol{r} r^2\rho \tag{3.26}$$

with respect to arbitrary variations of the proton and neutron densities and of the meson fields. The densities, fields and energy obtained from the solution of the variational equations associated to (3.26), now depend on the value of the parameter η. The nuclear r.m.s. radius is calculated as

$$R_\eta = \left[\frac{1}{A}\int d\boldsymbol{r} r^2\rho\right]^{1/2}, \tag{3.27}$$

where A is the mass number of the nucleus.

The constrained energy $E(\eta)$ has a minimum at $\eta = 0$ which corresponds to the ground-state r.m.s. radius R_0. Following Refs. [12,13,14,15] one expands $E(\eta)$ in a harmonic approximation about R_0 to obtain the constrained incompressibility of the finite nucleus as

$$K_{\rm A}^{\rm c} = \frac{1}{A} R_0^2 \left.\frac{\partial^2 E(\eta)}{\partial R_\eta^2}\right|_{\eta=0}. \tag{3.28}$$

In the constrained model the displacement field is also given by Eq. (3.20); now with a transition density $\rho_{\rm T}(r) = d\rho(r,\eta)/ds|_{\eta=0}$, where $s = R_\eta/R_0 - 1$ denotes the collective

variable of the constrained monopole oscillation [12,13,15]. The frequency of the constrained isoscalar monopole vibration is computed as

$$\bar{E}^{\rm c}_{\rm M} = \sqrt{\frac{AK^{\rm c}_{\rm A}}{B^{\rm c}_{\rm M}}}. \tag{3.29}$$

Again, we may notice that if in this equation the inertia parameter is replaced by its non-relativistic limit $B^{\rm nr}_{\rm M}$, the energy of the constrained monopole vibration can be nominally written in terms of sum rules. In the present case one hase $\bar{E}^{\rm c}_{\rm M} = \sqrt{m_1/m_{-1}}$, with m_{-1} being the inverse energy-weighted sum rule

$$m_{-1} = -\frac{1}{2} A \left.\frac{\partial R^2_\eta}{\partial \eta}\right|_{\eta=0} = \frac{1}{2} \left.\frac{\partial^2 E(\eta)}{\partial \eta^2}\right|_{\eta=0}. \tag{3.30}$$

3.5 Numerical results

Our RTF and RETF results for the excitation energy of the isoscalar giant monopole resonance (GMR) obtained in the scaling approach are displayed in Table 1, together with the empirical estimate $E_{\rm x} \sim 80/A^{1/3}$ MeV [41]. We have considered the nuclei ^{40}Ca, ^{90}Zr, ^{116}Sn, ^{144}Sm and ^{208}Pb for which recent experimental data on the GMR are available [42], in addition to ^{16}O and ^{48}Ca. We have employed the non-linear parameter sets NL1 (incompressibility $K_\infty = 211$ MeV, effective mass in nuclear matter $m^*_\infty/m = 0.57$) [43], NL3 [4] ($K_\infty = 272$ MeV, $m^*_\infty/m = 0.60$), NL-SH [44] ($K_\infty = 355$ MeV, $m^*_\infty/m = 0.60$) and NL2 [45] ($K_\infty = 399$ MeV, $m^*_\infty/m = 0.67$). The predictive power of these parametrizations is well known and some examples can be found, e.g., in Ref. [46] and references quoted therein. The relatively new parameter set NL3 is considered to be the most successful relativistic effective interaction so far. It is to be noted that the RMF parameter sets are determined by least-squares fits to ground-state properties like radii, binding energies and spin-orbit splittings of a few spherical nuclei. Then, there is no further adjustment to be made in the parameters of the interaction.

From Table 1 we see that the smaller the mass number, the larger is the monopole excitation energy. The energy of the GMR increases with increasing K_∞ in the various parameter sets. For example, in the RETF calculation the excitation energy for ^{208}Pb is 12.7 MeV with NL1, while it is 18.4 MeV with NL2. At first glance the dependence on K_∞

is roughly linear for each nucleus. We realize that, overall, the importance of the gradient corrections of order $\hbar^2$ included in the RETF approach is small for the GMR energy: the RETF energies differ by less than 10% from the RTF energies. The largest deviations between the RETF and RTF results are found for the lighter systems, where the surface terms are comparatively more important. If we analyze the relative difference between the RETF and RTF energies it is seen to decrease with increasing mass number in all sets, with the sole exception of ^{16}O with NL3. For example, the difference goes from -7% in ^{16}O to -1.6% in ^{208}Pb with NL1. We observe that the sign of the correction to the energy of the monopole state due to the $\hbar^2$ terms depends on the value of K_∞. In the case of NL1 the change of RETF with respect to RTF is negative. For NL3 and NL-SH the change becomes more and more positive with K_∞ (the effective mass m^*_∞/m of these two sets being almost the same). When we look at NL2 the change is again positive, but smaller in relative value than for NL-SH owing to the larger effective mass of NL2, which tends to counterbalance the effect of K_∞.

It is usually recognized that microscopic calculations of the isoscalar GMR energy in nuclei provide a reliable source of information on the nuclear matter incompressibility K_∞ [47,48]. The value of K_∞ is an important ingredient not only for the description of finite nuclei but also for the study of heavy ion collisions, supernovae and neutron stars. In practice one has several effective interactions which differ mostly by their prediction for K_∞, but otherwise reproduce satisfactorily the experimental data on ground-state properties. Comparison of the calculated GMR energies with experiment restricts the range of acceptable values for the nuclear matter incompressibility of the effective nuclear force. From Table 1 we see that the empirical law $E_{\rm x} \sim 80/A^{1/3}$ MeV roughly lies in between the predictions of the NL1 and NL3 parameter sets, as expected from the reasonable value of K_∞ in these interactions. On the contrary, the NL-SH and NL2 parametrizations have too high a value of K_∞ and clearly overestimate the empirical curve and the experimental data for all the considered nuclei. In Figure 1 we have drawn further RETF results for the excitation energy of the monopole mode in comparison with the experimental data listed in Ref. [49], as a function of the number of particles of the nucleus. (The RTF calculation displays basically

the same trend as the RETF results.) Again, it is clear that the NL-SH and NL2 sets are unable to describe the experimental values. The experimental points are roughly enclosed within the predictions of the NL1 and NL3 sets. For medium mass nuclei NL1 is closer to experiment than NL3, while for heavier nuclei the experimental energies tend to approach the results obtained with NL3.

A further inspection of Table 1 shows that no RMF parameter set seems capable of reproducing the mass-number dependence of the experimental data over the whole analyzed region, particularly in the lighter nuclei. One should note, however, that the scaling calculation provides a prediction for the mean value or centroid of the excitation energy of the resonance. To establish a relation between the incompressibility K_∞ and the experimentally measured energies of the monopole mode the most favourable situation is met in heavy nuclei, where the strength of the GMR is less fragmented than in medium and light nuclei [42,49]. If we take into account the excitation energies of ^{116}Sn, ^{144}Sm and ^{208}Pb, according to Table 1 the nuclear matter incompressibility K_∞ of the relativistic interaction should lie in the range 220–260 MeV. If we only consider ^{144}Sm and ^{208}Pb, as in Ref. [20], then K_∞ would be restricted to the range 230–260 MeV. For comparison, the authors of Refs. [11,20] conclude that the value of K_∞ should be close to 250–270 MeV from their time-dependent RMF and relativistic RPA calculations. The analysis of the relativistic RPA peak energies reported in Ref. [9] for ^{208}Pb suggests instead a range 235–250 MeV for K_∞. On the other hand, non-relativistic Hartree–Fock plus RPA analyses using Skyrme and Gogny interactions determine K_∞ to be 215 ± 15 MeV [47,48], thus lower than in the RMF model.

The restoring force $C_{\rm M}$ of the GMR defines the incompressibility $K_A^{\rm s}$ of the finite nucleus in the scaling model through $C_{\rm M} = AK_A^{\rm s}$. In the limit of an arbitrarily large nucleus $K_A^{\rm s}$ should approach the nuclear matter value K_∞, see Eq. (3.16). This suggests a linear dependence of the incompressibility of finite nuclei on the bulk incompressibility K_∞ of the effective interaction. In Figure 2 we display the value of $K_A^{\rm s}$ for the nuclei ^{16}O, ^{40}Ca, ^{116}Sn and ^{208}Pb obtained from our RETF calculation, as a function of K_∞. Apart from the parameter sets discussed in Table 1, we have employed the sets NL-Z, LZ, L1, L2, L3 and

HS compiled in Table 3 of Ref. [50], the sets NLB, NLC and NLD from Ref. [51], NL-RA1 from Ref. [52] and L0 from Ref. [43]. The bulk incompressibility of these sets spans a wide range of values, from ~ 175 to 625 MeV. The sets L0, LZ, L1, L2, L3 and HS correspond to the linear model without scalar self-interactions.

The results of Figure 2 show a remarkable linear behaviour of $K_A^{\rm s}$ with the compression modulus K_∞. This is more true for the heavier systems on the one hand, and for the non-linear parameter sets on the other hand. The linear sets show a considerable dispersion, but one should take into account that only L0 and LZ were optimally adjusted to nuclear ground-state properties and that, furthermore, L1, L2 and L3 do not include the ρ field. The incompressibilities of ^{208}Pb and ^{116}Sn are nearly the same. To see a perceptible change one has to go to ^{40}Ca. In Figure 3 we have drawn the excitation energy $\bar{E}_{\rm M}^{\rm s}$ of the monopole state versus the K_∞ incompressibility. As expected from the pattern displayed by $K_A^{\rm s}$, the monopole excitation energy increases smoothly with the bulk compression modulus, roughly as a linear function of the square root of K_∞ (in agreement, e.g., with Refs. [9,47]). Both the effective mass at saturation m_∞^* and the mass of the scalar meson $m_{\rm s}$ play a major role in the determination of the nuclear structure properties in the RMF theory. The effective mass has a direct influence on the spin–orbit force and the single-particle levels, while the scalar mass is related with the range of the attractive part of the effective nuclear force and thus strongly affects the nuclear surface. One may wonder whether these two quantities have some effect on the energy of the breathing mode. Figure 4 shows that this is not the case, as no evident correlation seems to exist between $\bar{E}_{\rm M}^{\rm s}$ and the value of m_∞^* or $m_{\rm s}$.

From the data represented in Figure 2 we obtain the relations

$$\begin{aligned}
K_A^{\rm s} &= 0.66K_\infty - 12 \text{ MeV} \qquad \text{for } ^{208}\text{Pb}, \\
K_A^{\rm s} &= 0.65K_\infty - 9 \text{ MeV} \qquad \text{for } ^{116}\text{Sn}, \\
K_A^{\rm s} &= 0.57K_\infty - 7 \text{ MeV} \qquad \text{for } ^{40}\text{Ca}, \\
K_A^{\rm s} &= 0.45K_\infty - 8 \text{ MeV} \qquad \text{for } ^{16}\text{O}.
\end{aligned} \tag{3.31}$$

The expressions for oxygen and calcium are not as meaningful as for the heavier nuclei, and we give them mostly for the purpose of illustration. Though there is a dependence on the mass number, the slope of the linear fits (3.31) is visibly smaller than unity. Moreover,

we have obtained a non-vanishing constant term. This is consistent with the leptodermous expansion of the incompressibility of a finite nucleus, inspired from the liquid drop formula, in which one separates the volume, surface, symmetry, Coulomb and higher-order contributions by writing

$$K_A^{\rm s} = K_\infty + K_{\rm surf}^{\rm s}/A^{1/3} + K_{\rm sym}(N-Z)^2/A^2 + K_{\rm Coul}Z^2/A^{4/3} + \cdots . \qquad (3.32)$$

The total incompressibility $K_A^{\rm s}$ receives a sizeable contribution from the surface term and smaller contributions from the symmetry and Coulomb terms [18,53]. The sign of these terms is negative and they considerably decrease the value of $K_A^{\rm s}$ in real nuclei with respect to the K_∞ limit [17,18,53,54]. A key point is the fact that the surface incompressibility $K_{\rm surf}^{\rm s}$ in the scaling model varies almost as a linear function of K_∞, which guarantees that the surface effects do not destroy the regular behaviour of $K_A^{\rm s}$ with K_∞. For instance, our RETF calculations of the $K_{\rm surf}^{\rm s}$ coefficient for several relativistic parameter sets [55], by using the scaling method in semi-infinite nuclear matter, confirm that $K_{\rm surf}^{\rm s}$ in the relativistic model indeed behaves roughly linearly with the bulk compression modulus, as happens with non-relativistic Skyrme forces. In fact we have found [55] that the rule of thumb $K_{\rm surf}^{\rm s} \sim -K_\infty$ known from the non-relativistic approach [54], also applies to non-linear RMF parameter sets having not too large values of the compression modulus. In the case of the linear $\sigma-\omega$ sets, which have a high K_∞ value, one instead finds $K_{\rm surf}^{\rm s} \sim -1.5K_\infty$.

It is interesting to compare (3.31) with the equations $K_A^{\rm s} = 0.62K_\infty + 23$ MeV for ^{208}Pb and $K_A^{\rm s} = 0.49K_\infty + 35$ MeV for ^{40}Ca obtained in Ref. [56] from an analysis of the scaling incompressibility performed with the Skyrme forces SkM*, SGI and SIII. In the relativistic model the independent term of the linear fits is negative and seems to be more constant with mass number, but the coefficient in front of K_∞ is similar in both the relativistic and non-relativistic model. The authors of Ref. [56] signaled that the slope obtained for ^{208}Pb with the Skyrme forces approaches the hydrodynamical value $\pi^2/15 = 0.658$, though they stressed that this might be just accidental. It is at least curious to come across with the same value in the relativistic model.

In assuming a nuclear matter approach Nishizaki et al. [31] estimated the monopole

excitation energy of a finite nucleus in the relativistic model as

$$\bar{E}^{\rm s}_{\rm M} = \sqrt{\frac{K_\infty}{\mu_\infty \langle r^2 \rangle}}, \tag{3.33}$$

where μ_∞ is the chemical potential of nuclear matter (including the nucleon rest mass), $\langle r^2 \rangle = \frac{3}{5}R^2$ and $R = 1.2A^{1/3}$ fm. They evaluated (3.33) for the linear model of Walecka using $\mu_\infty = 923$ MeV and $K_\infty = 525$ MeV and found $\bar{E}^{\rm s}_{\rm M} = 160/A^{1/3}$ MeV. This result has the correct dependence on the mass number but it is twice as large as the empirical value $\sim 80/A^{1/3}$ MeV. Calculating (3.33) for the non-linear parametrizations NL1, NL3, NL-SH and NL2 one finds $\bar{E}^{\rm s}_{\rm M} = 102$, 115, 132, and $140/A^{1/3}$ MeV, respectively. Compared to the empirical law these values are too large by a factor ~ 1.5–1.8, depending on the compression modulus of the force. If we furthermore compare with the results of the calculations for finite nuclei listed in Table 1, we realize that the finite size effects reduce the prediction obtained from nuclear matter by a factor ranging from 1.6 in ^{16}O to 1.3 in ^{208}Pb, almost independently of the parameter set.

In a recent work Piekarewicz [9] has given a thorough presentation of the relativistic RPA formalism and has computed the isoscalar monopole mode for several closed-shell nuclei. In the numerical calculations he has used the non-linear sets NLC and NLB and the linear set L2′, which have the nuclear matter incompressibilities $K_\infty = 224$, 421 and 547 MeV, respectively. We present in Table 2 our values obtained from the scaling method versus the RRPA peak energies of the isoscalar mode taken from Ref. [9], for the systems ^{40}Ca, ^{90}Zr and ^{208}Pb. A fairly good agreement is found between our semiclassical calculations and the more fundamental RRPA approach. The differences are well below 5% in ^{208}Pb and, excluding the RETF result for ^{40}Ca with L2′, below 10% in ^{40}Ca and ^{90}Zr. As discussed in Ref. [9], it becomes difficult to even identify a genuine resonance in the RRPA distribution of the isoscalar monopole strength for medium-size nuclei such as ^{40}Ca with the parameter sets NLB and L2′ which have large compression moduli.

The GMR has also been studied by means of constrained calculations in the RMF model and, based upon them, with the more ellaborate generator coordinate method (GCM). The constrained calculations in our semiclassical approach (see Section 3.4) are carried out in a similar way to that of Refs. [12,13,14,15] within the quantal Hartree approach. We report in

Table 3 the excitation energies of ^{16}O, ^{40}Ca, ^{90}Zr and ^{208}Pb calculated with the constrained RETF method (for the NL1, NL2, NL3 and NL-SH sets), besides the constrained RMF (CRMF) Hartree results of Ref. [14] and the GCM results of Ref. [11]. In non-relativistic RPA calculations it is common to utilize the moments m_k of the strength function to analyze the monopole resonance [19]. The lowest moments correspond to simple sum rules and in the limit of small amplitude oscillations the ratios $\sqrt{m_3/m_1}$ and $\sqrt{m_1/m_{-1}}$ can be identified, respectively, with the scaling and constrained monopole excitation energies [18,47,57].

We see that the excitation energies of the monopole state are smaller in the constrained model (Table 3) than in the scaling model (Table 1). This is in agreement with the non-relativistic RPA inequality $\sqrt{m_1/m_{-1}} \leq \sqrt{m_3/m_1}$ [19]. When the comparison is possible, the energies obtained with the GCM are systematically smaller than in the CRMF Hartree model, which in turn are smaller than in the constrained RETF approach. The constrained RETF values agree very well with the GCM and CRMF values for NL1, but the agreement worsens for light nuclei with the other parameter sets. In the case of ^{208}Pb, for which the semiclassical technique should work better, the constrained RETF calculation overestimates the GCM value by around 1 MeV, the same magnitude by which the CRMF and GCM results differ (for NL1 and NL-SH).

Vretenar et al. [11] have studied the GMR with the time-dependent RMF approach. (We recall that very recently it has been demonstrated that the relativistic RPA, with inclusion of Dirac sea states, is equivalent to the small amplitude limit of the time-dependent RMF theory in the no-sea approximation [20].) In the calculations of Ref. [11] the main peak appearing in the monopole strength distribution of ^{208}Pb has energies 12.4 (NL1), 14.1 (NL3), 16.1 (NL-SH) and 17.8 MeV (NL2), while in the case of ^{90}Zr the energies are 15.7 (NL1) and $\sim$ 18 MeV (NL3). For ^{208}Pb our scaling results (cf. Table 1) show a good agreement in all the parameter sets. In fact, if we focus on the RETF values, we see that the scaling energies are an upper bound of the time-dependent RMF energies, while the constrained energies of Table 3 represent a lower bound (apart from the case of NL-SH by a little deviation). For ^{90}Zr, however, both the scaling and constrained semiclassical excitation energies are larger than those of Ref. [11]. It should be pointed out that the Fourier spectrum

of ^{90}Zr in the time-dependent RMF calculation is considerably fragmented (specially for the sets with higher K_∞) and then the determination of the centroid energy remains more uncertain [11].

4 Giant quadrupole resonance

In the quadrupole vibration the particle density scales as [19]

$$\rho_\lambda(\boldsymbol{r}) = \rho(x/\lambda, y/\lambda, \lambda^2 z). \tag{4.1}$$

While the volume element is conserved in both coordinate and momentum space, the momentum distribution, which remained spherically symmetric in the monopole oscillation, becomes highly deformed in the quadrupole case [6,58]:

$$\boldsymbol{p}_\lambda = (\lambda p_x, \lambda p_y, p_z/\lambda^2). \tag{4.2}$$

One has to note that the spherically averaged form of the distribution function $\mathcal{R}(\boldsymbol{r}, \boldsymbol{p})$ cannot be employed in the quadrupole scaling calculations due to the deformation of the Fermi sphere [58]. This means, in particular, that the spherically symmetric expressions (2.4), (2.5) and (2.12) of the semiclassical energy density and scalar density are no longer valid for use in the quadrupole scaling. That is, first, one should replace $\boldsymbol{p}$ by $\boldsymbol{p}_\lambda$ in the semiclassical expansion of the relativistic distribution function $\mathcal{R}(\boldsymbol{r}, \boldsymbol{p})$ [34] and then obtain its moments (energy and densities) as a function of the collective coordinate λ. This extraordinarily complicates the expressions if the distribution function with terms up to order $\hbar^2$ is to be used. Since the final magnitude of the contribution of the $\hbar^2$-order corrections in the semiclassical calculation of the excitation energy of giant resonances is not very significant, we will work at the Thomas–Fermi level in the present study of the giant quadrupole resonance.

In the Thomas–Fermi approach the relativistic distribution function is proportional to a step function (Appendix A and Ref. [34]), which vanishes for single-particle energies above the Fermi level. The Thomas–Fermi energy density of the non-linear $\sigma - \omega$ model after scaling then reads

$$\begin{aligned}\mathcal{H}_\lambda &= \frac{2}{(2\pi)^3}\sum_q \int d\boldsymbol{p}\, \sqrt{p_\lambda^2 + m_\lambda^{*\,2}}\; \Theta\left(\mu_{q\lambda} - \sqrt{p_\lambda^2 + m_\lambda^{*\,2}} - u_{q\lambda}\right) \\ &\quad + \frac{1}{2} g_{\rm s}\phi_\lambda \rho_{{\rm s}\lambda}^{\rm eff} + \frac{1}{3} b\phi_\lambda^3 + \frac{1}{4} c\phi_\lambda^4 + \frac{1}{2} g_{\rm v} V_\lambda \rho_\lambda + \frac{1}{2} g_\rho R_\lambda \rho_{3\lambda} + \frac{1}{2} e\mathcal{A}_\lambda \rho_{{\rm p}\lambda},\end{aligned} \tag{4.3}$$

where Θ denotes the step function, $\mu_{q\lambda}$ is the chemical potential of the scaled system for each kind of nucleon and the single-particle potential $u_{q\lambda}$ is given by

$$u_{q\lambda} = g_{\rm v} V_\lambda + \frac{1}{2} g_\rho R_\lambda \tau_3 + \frac{1}{2} e \mathcal{A}_\lambda (1+\tau_3). \tag{4.4}$$

The scaled effective scalar density $\rho_{{\rm s}\lambda}^{\rm eff}$ has been defined through

$$\begin{aligned} g_{\rm s}\rho_{{\rm s}\lambda}^{\rm eff} &= g_{\rm s}\rho_{{\rm s}\lambda} - b\phi_\lambda^2 - c\phi_\lambda^3 \\ &= \frac{2}{(2\pi)^3}\sum_q \int d\boldsymbol{p}\, \frac{g_{\rm s} m_\lambda^*}{\sqrt{p_\lambda^2 + {m_\lambda^*}^2}}\, \Theta\left(\mu_{q\lambda} - \sqrt{p_\lambda^2 + {m_\lambda^*}^2} - u_{q\lambda}\right) - b\phi_\lambda^2 - c\phi_\lambda^3. \end{aligned} \tag{4.5}$$

The position and momentum variables in these expressions scale according to the rules (4.1) and (4.2) in the quadrupole case.

To obtain the restoring force $C_{\rm Q}$ of the quadrupole oscillation we have to compute the second derivative of the scaled energy with respect to the collective coordinate λ. The first derivative reads

$$\begin{aligned} &\frac{\partial}{\partial\lambda}\int d\boldsymbol{r}\mathcal{H}_\lambda(\boldsymbol{r}) = \\ &\int d\boldsymbol{r}\left[\frac{2}{(2\pi)^3}\sum_q \int d\boldsymbol{p}\, \frac{p_\lambda}{\sqrt{p_\lambda^2 + {m_\lambda^*}^2}}\frac{\partial p_\lambda}{\partial\lambda}\, \Theta\left(\mu_{q\lambda} - \sqrt{p_\lambda^2 + {m_\lambda^*}^2} - u_{q\lambda}\right) - g_{\rm s}\rho_{{\rm s}\lambda}^{\rm eff}\frac{\partial\phi_\lambda}{\partial\lambda}\right] \\ &+ \frac{\partial}{\partial\lambda}\int d\boldsymbol{r}\left[\frac{1}{2}g_{\rm s}\phi_\lambda\rho_{{\rm s}\lambda}^{\rm eff} + \frac{1}{2}g_{\rm v}V_\lambda\rho_\lambda + \frac{1}{2}g_\rho R_\lambda\rho_{3\lambda} + \frac{1}{2}e\mathcal{A}_\lambda\rho_{{\rm p}\lambda}\right]. \end{aligned} \tag{4.6}$$

It can be checked that this equation identically vanishes at $\lambda = 1$, as in the non-relativistic case [19]. Before deriving again (4.6) it is helpful to take into account that, for instance,

$$\begin{aligned} &\int d\boldsymbol{r}\rho_\lambda(\boldsymbol{r})V_\lambda(\boldsymbol{r}) = \int d\boldsymbol{r}\rho\Big(\frac{x}{\lambda},\frac{y}{\lambda},\lambda^2 z\Big)\int d\boldsymbol{r}'\rho\Big(\frac{x'}{\lambda},\frac{y'}{\lambda},\lambda^2 z'\Big)\frac{g_{\rm v}}{4\pi}\frac{e^{-m_{\rm v}|\boldsymbol{r}-\boldsymbol{r}'|}}{|\boldsymbol{r}-\boldsymbol{r}'|} = \\ &\int d\boldsymbol{r}\rho(\boldsymbol{r})\int d\boldsymbol{r}'\rho(\boldsymbol{r}')\mathcal{V}_\omega(s_\lambda), \end{aligned} \tag{4.7}$$

where

$$\mathcal{V}_\omega(s_\lambda) = \frac{g_{\rm v}}{4\pi}\frac{e^{-m_{\rm v}s_\lambda}}{s_\lambda}, \qquad \boldsymbol{s}_\lambda = (\lambda x - \lambda x', \lambda y - \lambda y', z/\lambda^2 - z'/\lambda^2). \tag{4.8}$$

With this, after some algebra, the restoring force of the quadrupole mode can be put in the form

$$C_{\rm Q} = \left[\frac{\partial^2}{\partial\lambda^2}\int d\boldsymbol{r}\mathcal{H}_\lambda(\boldsymbol{r})\right]_{\lambda=1} =$$

$$\int d\boldsymbol{r}\Bigg\{\frac{2}{(2\pi)^3}\sum_q\int d\boldsymbol{p}\left[\frac{p_x^2+p_y^2+10p_z^2}{(p^2+m^{*2})^{1/2}}-\frac{(p_x^2+p_y^2-2p_z^2)^2}{(p^2+m^{*2})^{3/2}}\right]\Theta(p-p_{\mathrm{F}q})$$

$$+\,g_{\mathrm{s}}\left.\frac{\partial\rho^{\mathrm{eff}}_{\mathrm{s}\lambda}}{\partial\lambda}\right|_{\lambda=1}\int d\boldsymbol{r}'\rho^{\mathrm{eff}}_{\mathrm{s}}(\boldsymbol{r}')\frac{1}{s}\frac{d\mathcal{V}_\sigma}{ds}s_-^2-\frac{1}{2}g_{\mathrm{s}}\rho^{\mathrm{eff}}_{\mathrm{s}}\int d\boldsymbol{r}'\rho^{\mathrm{eff}}_{\mathrm{s}}(\boldsymbol{r}')\left[\frac{1}{s}\frac{d}{ds}\left(\frac{1}{s}\frac{d\mathcal{V}_\sigma}{ds}\right)s_-^4+\frac{3}{s}\frac{d\mathcal{V}_\sigma}{ds}s_+^2\right]$$

$$+\,\frac{1}{2}g_{\mathrm{v}}\rho\int d\boldsymbol{r}'\rho(\boldsymbol{r}')\left[\frac{1}{s}\frac{d}{ds}\left(\frac{1}{s}\frac{d\mathcal{V}_\omega}{ds}\right)s_-^4+\frac{3}{s}\frac{d\mathcal{V}_\omega}{ds}s_+^2\right]$$

$$+\,\frac{1}{2}g_\rho\rho_3\int d\boldsymbol{r}'\rho_3(\boldsymbol{r}')\left[\frac{1}{s}\frac{d}{ds}\left(\frac{1}{s}\frac{d\mathcal{V}_\rho}{ds}\right)s_-^4+\frac{3}{s}\frac{d\mathcal{V}_\rho}{ds}s_+^2\right]+\frac{1}{2}e\rho_{\mathrm{p}}\int d\boldsymbol{r}'\rho_{\mathrm{p}}(\boldsymbol{r}')\frac{3e}{4\pi}\left(\frac{s_-^4}{s^5}-\frac{s_+^2}{s^3}\right)\Bigg\},\tag{4.9}$$

where we have set $s_\mp^2=s_x^2+s_y^2\mp 2s_z^2$.

After performing the angular average in the integral over $\boldsymbol{p}$ and in the integrals over $\boldsymbol{r}$ and $\boldsymbol{r}'$, we finally get

$$\begin{aligned}C_{\mathrm{Q}} &= \frac{2}{5}\int d\boldsymbol{r}\Bigg\{\frac{2}{\pi^2}\left[\frac{k_{\mathrm{Fn}}^5}{\epsilon_{\mathrm{Fn}}}+\frac{k_{\mathrm{Fp}}^5}{\epsilon_{\mathrm{Fp}}}\right]-g_{\mathrm{s}}\rho^{\mathrm{eff}}_{\mathrm{s}}\int d\boldsymbol{r}'\rho^{\mathrm{eff}}_{\mathrm{s}}(\boldsymbol{r}')\left[4s\frac{d\mathcal{V}_\sigma}{ds}+s^2\frac{d^2\mathcal{V}_\sigma}{ds^2}\right]\\ &\quad+g_{\mathrm{v}}\rho\int d\boldsymbol{r}'\rho(\boldsymbol{r}')\left[4s\frac{d\mathcal{V}_\omega}{ds}+s^2\frac{d^2\mathcal{V}_\omega}{ds^2}\right]\\ &\quad+g_\rho\rho_3\int d\boldsymbol{r}'\rho_3(\boldsymbol{r}')\left[4s\frac{d\mathcal{V}_\rho}{ds}+s^2\frac{d^2\mathcal{V}_\rho}{ds^2}\right]-2e\mathcal{A}\rho_{\mathrm{p}}\Bigg\}.\end{aligned}\tag{4.10}$$

As far as the nuclear part is concerned this result coincides with the one derived in Ref. [31] for nuclear matter using a local Lorentz boost and the scaling method. The contributions from the meson fields agree with the result obtained from the potential part of an effective density-independent nuclear force in the non-relativistic model [57] (and the contribution from the Coulomb field agrees with that given in Ref. [19]).

As in the monopole oscillation to calculate the mass parameter one needs the continuity equation in a moving frame, Eq. (A.15). For the quadrupole vibration we have $\rho_\lambda(\boldsymbol{r})=\rho(x/\lambda,y/\lambda,\lambda^2 z)$ and the continuity equation (A.15) is fulfilled by $\boldsymbol{v}=-\dot\lambda(-x,-y,2z)=-\dot\lambda\boldsymbol{\nabla}[\sqrt{4\pi/5}r^2Y_{20}(\Omega)]$ at $\lambda=1$ [31], which provides the connection between the velocity of the moving frame and the collective coordinate. Proceeding similarly to the monopole case, i.e., inserting this velocity field into Eq. (A.13) and taking the second derivative with

respect to $\dot{\lambda}$, the mass parameter of the quadrupole mode is found to be

$$B_{\rm Q} = 2 \int d\boldsymbol{r} r^2 \mathcal{H}, \tag{4.11}$$

assuming the nucleus to be spherical. The excitation energy of the quadrupole state then is

$$\bar{E}^{\rm s}_{\rm Q} = \sqrt{\frac{C_{\rm Q}}{B_{\rm Q}}}. \tag{4.12}$$

The transition density in the quadrupole case is given by

$$\rho_{\rm T}(\boldsymbol{r}) = \left.\frac{d\rho_\lambda(\boldsymbol{r})}{d\lambda}\right|_{\lambda=1} = \boldsymbol{\nabla}\rho_\lambda(\boldsymbol{r})|_{\lambda=1} \cdot \boldsymbol{\nabla}[\sqrt{4\pi/5} r^2 Y_{20}(\Omega)] = \sqrt{\frac{16\pi}{5}} r \frac{d\rho(r)}{dr} Y_{20}(\Omega), \tag{4.13}$$

where again we have assumed the density to be spherically symmetric at $\lambda = 1$.

4.1 Numerical results

As we have indicated, our calculations for the quadrupole mode are restricted to the RTF approximation. We collect in Table 4 the calculated excitation energy of the quadrupole oscillation for ^{16}O, ^{40}Ca, ^{48}Ca, ^{90}Zr and ^{208}Pb, along with the empirical law $E_{\rm x} \sim 65/A^{1/3}$ MeV and some experimental data taken from Ref. [41]. The theoretical results shown in this table correspond to the non-linear sets NL1, NL3, NL-SH and NL2, and to the set LZ ($K_\infty = 586$ MeV, $m^*_\infty/m = 0.53$) which we take as a representative of the linear sets.

One can see that the four non-linear $\sigma - \omega$ parametrizations reproduce the empirical trend and that, contrary to the situation found in the monopole case, they give rather similar results for each nucleus. This is due to the fact that the energy of the quadrupole vibration is basically independent of the bulk compression modulus of the effective force. Nevertheless, the comparison with experiment favours the NL3 set and, especially, the NL1 set (i.e., those sets with a lower incompressibility). In fact, if the incompressiblity of the force is very large (set LZ) the theoretical predictions clearly overestimate the experimental values. The relativistic results of the non-linear sets compare well with those obtained in non-relativistic Hartree–Fock and extended Thomas–Fermi calculations using Skyrme forces [26]. Calculations of the isoscalar giant quadrupole resonance are rather scarce in the relativistic domain. Time-dependent RMF calculations of this mode have been carried out

in Ref. [10] using the NL-SH parameter set. Our relativistic Thomas–Fermi calculation is in good agreement with the excitation energies of 23.6, 17.7 and 17.7 MeV for ^{16}O, ^{40}Ca and ^{48}Ca, respectively, reported in that work.

The energy of the quadrupole excitation has also been evaluated by Nishizaki et al. [31] from a nuclear matter approach as

$$\bar{E}^{\rm s}_{\rm Q} = \sqrt{\frac{6k^2_{{\rm F},\infty}}{5\epsilon_{{\rm F},\infty}\mu_\infty\langle r^2\rangle}}, \tag{4.14}$$

where $\langle r^2\rangle$ has been defined in Eq. (3.33). In this approximation the restoring force of the quadrupole vibration corresponds to the nuclear matter limit of Eq. (4.10), where all the terms with derivatives of the meson fields vanish and only the first term survives. Note that the incompressibility K_∞ of the interaction does not enter Eq. (4.14). According to this equation one obtains $\bar{E}^{\rm s}_{\rm Q} = 85$, 84, 81, 80, and $76/A^{1/3}$ MeV for the LZ, NL1, NL3, NL-SH and NL2 sets, respectively. We thus see that in nuclear matter $\bar{E}^{\rm s}_{\rm Q}$ decreases as the value of the effective mass at saturation of the force (m^*_∞) increases. However, in the full RTF calculation for finite nuclei (Table 4) the regular pattern of $\bar{E}^{\rm s}_{\rm Q}$ with m^*_∞ observed in nuclear matter is destroyed by the finite size effects. In the case of finite systems one not only has the additional contribution from the meson fields into Eq. (4.10), but also the nuclear part is modified by the shape of the nuclear surface, this one depending in turn on the mass of the sigma meson $m_{\rm s}$. Such effects mask the simple relation of $\bar{E}^{\rm s}_{\rm Q}$ with m^*_∞ shown by the naive nuclear matter approximation.

5 Summary and conclusions

We have studied the isoscalar giant monopole and quadrupole resonances of finite nuclei by means of the scaling method and the Thomas–Fermi and extended Thomas–Fermi approaches to relativistic mean field theory. Self-consistent numerical calculations for realistic non-linear $\sigma - \omega$ parameter sets have been discussed. Previous relativistic investigations with the scaling method either relied on a leptodermous expansion of the finite nucleus incompressibility [15,16,17], or were limited to the linear $\sigma - \omega$ model for symmetric and uncharged nuclei at the Thomas–Fermi level [31,32].

In the present approach one starts by scaling the spatial and momentum coordinates of the semiclassical distribution function in a moving frame. By taking the derivatives of the scaled energy in the moving frame with respect to the collective coordinate and the collective velocity, one obtains the expressions from which the restoring force and the mass parameter of the resonance can be computed. The underlying reason for the success of the method is that in the semiclassical approach the energy functional is written explicitly in terms of the local Fermi momentum *and* of the local effective mass, which allows one to easily perform the scaling. Due to the finite range of the relativistic interaction no compact formulas can be obtained as in the case of non-relativistic Skyrme forces. Nevertheless, the scaling excitation energies of the monopole and quadrupole resonances only depend on the ground-state densities and fields, which means that they can be computed as a by-product of a semiclassical self-consistent calculation of the ground state.

We have found that the total contribution to the excitation energy of the GMR coming from the gradient corrections of order $\hbar^2$, which are included in the RETF approach, does not modify the Thomas–Fermi result very much. The strength and sign of these corrections of order $\hbar^2$ is strongly correlated with the nuclear matter incompressibility and the effective mass at saturation of the relativistic interaction.

We have investigated the relation between the incompressibility $K_A^{\rm s}$ of finite nuclei in the scaling model and the compression modulus of nuclear matter K_∞, employing a variety of relativistic parameter sets. The dependence is roughly linear, as in non-relativistic analyses. Even a nucleus such as ^{208}Pb is not large enough to obtain a relation of propor-

tionality between $K_A^{\rm s}$ and K_∞. The excitation energy of the monopole oscillation increases smoothly with $K_\infty^{1/2}$, in correspondence with the behaviour of $K_A^{\rm s}$. No regular pattern of the monopole excitation energy with the mass of the scalar meson or with the effective mass of the interaction has been observed.

The experimental excitation energies of the monopole oscillation in medium and heavy nuclei lie in between the results obtained with the NL1 and NL3 parameter sets. An analysis of the calculated breathing-mode energies for ^{116}Sn, ^{144}Sm and ^{208}Pb, for which precise experimental data exist, predicts that the nuclear matter incompressibility should be around 220–260 MeV (230–260 MeV if only ^{144}Sm and ^{208}Pb are taken into account). A similar analysis carried out in Refs. [11,20] using time-dependent RMF and relativistic RPA results predicts a value slightly higher: 250–270 MeV. From the relativistic RPA peak energies given in Ref. [9] for ^{208}Pb we extract a range of 235–250 MeV. Thus, all these relativistic calculations point to a value of roughly 250 ± 20 MeV for K_∞, which is higher than the non-relativistic estimate of 215 ± 15 MeV from Skyrme and Gogny forces [47,48]. Relativistic parameter sets with large values of K_∞ (such as NL-SH or NL2), which may otherwise perform well in describing the data for nuclear masses and radii, should be discarded on the basis of the experimental information on breathing-mode energies.

The results computed with the scaling method represent an upper bound of the mean excitation energy of the GMR, to the extent that they are related with the cubic weighted sum rule. Instead, the breathing-mode energies obtained from constrained calculations rather represent a lower bound, since they are related with the inverse energy-weighted sum rule. Actually, with all the parameter sets and nuclei analyzed, we have found the calculated monopole energies to be larger in the scaling approach than in the constrained approach.

Our calculations of the excitation energy of the quadrupole oscillation have been restricted to the Thomas–Fermi approach, to simplify the problems related with the distortion of the Fermi sphere. All the considered non-linear parameter sets reproduce fairly well the empirical trend, rather independently of the value of the compression modulus of the force. Although a nuclear matter estimate predicts a decrease of the quadrupole excitation energy with an increase in the value of the effective mass at saturation, the finite size effects

and additional contributions from the meson fields mask this trend in the self-consistent calculations for actual nuclei.

In conclusion, we hope to have shown that the scaling method can be confidently used together with the relativistic Thomas–Fermi approach to estimate the excitation energy of the isoscalar monopole and quadrupole resonances in a simple and reliable way. The results for the breathing mode turn out to be in good agreement with the outcome of dynamical time-dependent RMF and relativistic RPA calculations. We can thus conclude that, similarly to the non-relativistic case, also in the relativistic framework the semiclassical excitation energies obtained with the scaling method simulate the results of the RPA. The method introduced in this work also allows one to self-consistently compute the surface incompressibility coefficient for relativistic interactions [55]. The study of other multipolarities using a generalized scaling simultaneously with the relativistic Thomas–Fermi approach may be a worthwhile task to pursue.

6 Acknowledgements

We thank Nguyen Van Giai for discussions and J. Navarro for carefully reading an earlier version of the manuscript and making a series of suggestions. Support from the DGICYT (Spain) under grant PB98-1247 and from DGR (Catalonia) under grant 2000SGR-00024 is acknowledged. S.K.P. thanks the Spanish Education Ministry grant SB97-OL174874 for financial support and the Departament d'Estructura i Constituents de la Matèria of the University of Barcelona for kind hospitality.

Appendix A

In this appendix we derive the Thomas–Fermi expression of the energy of a nucleus described by the non-linear $\sigma - \omega$ model in a frame moving with velocity $-\boldsymbol{v}$. As a final product we obtain general equations for the restoring force and the mass parameter of the giant resonance. For simplicity we shall consider an uncharged symmetric nucleus (the ρ meson field and the electromagnetic field behave like the vector field), and shall not include the corrections of order $\hbar^2$ to the Thomas–Fermi approximation.

The semiclassical expressions of densities and energies are most conveniently derived from the so-called phase-space distribution function [6]. For a Hamiltonian $\boldsymbol{\alpha}\cdot\boldsymbol{p} + \beta m^* + g_{\rm v}V$ the distribution function in Thomas–Fermi approximation reads [34]

$$\mathcal{R} = \frac{1}{2}\Theta(\mu - \epsilon - g_{\rm v}V)\left[I + \frac{1}{\epsilon}\{\boldsymbol{\alpha}\cdot\boldsymbol{p} + \beta m^*\}\right], \tag{A.1}$$

where μ is the chemical potential, $\epsilon = \sqrt{p^2 + m^{*2}}$ and I is the 4×4 unit matrix. Due to the step function in (A.1), p takes values from zero up to the Fermi momentum $p_{\rm F}$. The scalar field (ϕ) and the time-like component of the vector field (V) transform to a frame which moves with velocity $-\boldsymbol{v}$ like $\phi' = \phi$ and $V' = \gamma V$, with $\gamma = 1/\sqrt{1-v^2}$. The distribution function in the moving frame then is given by

$$\mathcal{R}' = \frac{1}{2}\Theta(\mu' - \epsilon' - \gamma g_{\rm v}V)\left[I + \frac{1}{\epsilon'}\{\boldsymbol{\alpha}\cdot(\boldsymbol{p}' - g_{\rm v}\boldsymbol{V}') + \beta m^*\}\right], \tag{A.2}$$

where μ' is the chemical potential in the new frame, $\epsilon' = \sqrt{(\boldsymbol{p}' - g_{\rm v}\boldsymbol{V}')^2 + m^{*2}}$, and we have defined

$$\boldsymbol{V}' \equiv \gamma\,\boldsymbol{v}V. \tag{A.3}$$

It is easy to see that $\Theta(\mu' - \epsilon' - \gamma g_{\rm v}V) = \Theta(\mu - \epsilon - g_{\rm v}V)$ $[\,= \Theta(p_{\rm F} - p)]$ by expressing ϵ' and μ' through their values in the rest frame:

$$\epsilon' = \gamma(\epsilon + \boldsymbol{p}\cdot\boldsymbol{v}), \qquad \mu' = \gamma(\mu + \boldsymbol{p}\cdot\boldsymbol{v}). \tag{A.4}$$

The baryon density in the moving frame is obtained as

$$\rho' = 2\int\frac{d\boldsymbol{p}'}{(2\pi)^3}{\rm Tr}[\,\mathcal{R}'\,] = 4\int\frac{d\boldsymbol{p}}{(2\pi)^3}\frac{\gamma}{\epsilon}(\epsilon + \boldsymbol{p}\cdot\boldsymbol{v})\Theta(p_{\rm F} - p) = \gamma\rho, \tag{A.5}$$

where we have taken into account that $d\boldsymbol{p}'/\epsilon' = d\boldsymbol{p}/\epsilon$ (Lorentz scalars) and the fact that the trace of the distribution function $\mathcal{R}'$ equals $2\Theta(p_{\rm F} - p)$. Similarly, the transformed scalar density is

$$\rho_{\rm s}' = 2\int \frac{d\boldsymbol{p}'}{(2\pi)^3}{\rm Tr}[\,\beta\mathcal{R}'\,] = 4\int \frac{d\boldsymbol{p}}{(2\pi)^3}\frac{m^*}{\epsilon}\Theta(p_{\rm F}-p) = \rho_{\rm s}. \tag{A.6}$$

The energy density in the moving frame is given by

$$\begin{aligned}\mathcal{H}' &= 2\int \frac{d\boldsymbol{p}'}{(2\pi)^3}{\rm Tr}[\,H'\mathcal{R}'\,] + \frac{1}{2}\left[(\boldsymbol{\nabla}'\phi)^2 + m_{\rm s}^2\phi^2\right] + \frac{1}{3}b\phi^3 + \frac{1}{4}c\phi^4 \\ &\quad - \frac{1}{2}\left[\gamma^2(\boldsymbol{\nabla}'V)^2 + \gamma^2 m_{\rm v}^2 V^2 - (\boldsymbol{\nabla}'\times\boldsymbol{V}')^2 - m_{\rm v}^2\boldsymbol{V}'^2\right],\end{aligned} \tag{A.7}$$

where $H' = \boldsymbol{\alpha}\cdot(\boldsymbol{p}' - g_{\rm v}\boldsymbol{V}') + \beta m^* + \gamma g_{\rm v} V$.

If spherical symmetry of the meson fields is assumed Eq. (A.7) becomes

$$\begin{aligned}\mathcal{H}' &= 4\int \frac{d\boldsymbol{p}}{(2\pi)^3}\frac{\gamma^2}{\epsilon}(\epsilon + \boldsymbol{p}\cdot\boldsymbol{v})(\epsilon + \boldsymbol{p}\cdot\boldsymbol{v} + g_{\rm v}V)\Theta(p_{\rm F}-p) \\ &\quad + \frac{1}{2}\left[(\boldsymbol{\nabla}\phi)^2 + m_{\rm s}^2\phi^2 + \frac{2}{3}\gamma^2 v^2(\boldsymbol{\nabla}\phi)^2\right] + \frac{1}{3}b\phi^3 + \frac{1}{4}c\phi^4 \\ &\quad - \frac{1}{2}\left[(\boldsymbol{\nabla}V)^2 + m_{\rm v}^2V^2 + \frac{2}{3}\gamma^2v^2(\boldsymbol{\nabla}V)^2\right].\end{aligned} \tag{A.8}$$

After integration over momentum, the relativistic energy density in the moving frame can be written as

$$\mathcal{H}' = \gamma^2\left\{\mathcal{H} + v^2\left[\rho\epsilon_{\rm F} + g_{\rm v}\rho V + \frac{1}{3}(\boldsymbol{\nabla}\phi)^2 - \frac{1}{3}(\boldsymbol{\nabla}V)^2 - \mathcal{H}\right]\right\}, \tag{A.9}$$

where $\mathcal{H}$ is the energy density in the rest frame (Section 2). Equation (A.9) agrees with the transformation law of the stress tensor as discussed in Ref. [59]. For a uniform system ($\boldsymbol{\nabla}\phi = \boldsymbol{\nabla}V = 0$) it also coincides with the result obtained in Ref. [31] from a local Lorentz boost.

Finally, the energy of the system in the moving frame is obtained by integrating (A.9) over the space. Taking into account the Lorentz contraction of the volume element, this yields

$$E(v) = \int \frac{d\boldsymbol{r}}{\gamma}\mathcal{H}' = \int d\boldsymbol{r}\gamma\left\{(1-v^2)\mathcal{H} + v^2\left[\rho\epsilon_{\rm F} + g_{\rm v}\rho V + \frac{1}{3}\left(\boldsymbol{\nabla}\phi\right)^2 - \frac{1}{3}\left(\boldsymbol{\nabla}V\right)^2\right]\right\}. \tag{A.10}$$

Combining this result with the meson field equations and the virial theorem derived in Appendix B, Eq. (B.10), the energy in the new frame reads

$$E(v) = \int d\boldsymbol{r}\gamma\{(1-v^2)\mathcal{H} + v^2\mathcal{H}\} = \int d\boldsymbol{r}\gamma\mathcal{H}. \tag{A.11}$$

The restoring force of the monopole and quadrupole oscillations is obtained by appropriately scaling the densities and mean fields in Eq. (A.11) and then computing the second derivative at $v = 0$ and $\lambda = 1$:

$$C = \left[\frac{\partial^2}{\partial\lambda^2}\int\frac{d\boldsymbol{r}}{\gamma}\mathcal{H}'_\lambda\right]_{v=0,\lambda=1} = \left[\frac{\partial^2}{\partial\lambda^2}\int d\boldsymbol{r}\mathcal{H}_\lambda\right]_{\lambda=1}, \tag{A.12}$$

where $\mathcal{H}'_\lambda$ and $\mathcal{H}_\lambda$ denote the scaled energy densities in the moving and rest frames, respectively. The mass or inertia parameter of the giant resonance is furnished by the second derivative of the scaled energy in the moving frame with respect to $\dot{\lambda} = d\lambda/dt$:

$$B = \left[\frac{\partial^2}{\partial\dot{\lambda}^2}\int\frac{d\boldsymbol{r}}{\gamma}\mathcal{H}'_\lambda\right]_{\dot{\lambda}=0,\lambda=1} = \left[\frac{\partial^2}{\partial\dot{\lambda}^2}\int d\boldsymbol{r}\gamma\mathcal{H}_\lambda\right]_{\dot{\lambda}=0,\lambda=1}. \tag{A.13}$$

To evaluate (A.13) it is necessary to relate the velocity $\boldsymbol{v}$ of the moving frame with the collective velocity $\dot{\lambda}$. This is achieved by scaling the continuity equation

$$\frac{\partial}{\partial t}\int\frac{d\boldsymbol{p}'}{\gamma(2\pi)^3}\mathrm{Tr}[\,\mathcal{R}'\,] + \boldsymbol{\nabla}\cdot\int\frac{d\boldsymbol{p}'}{\gamma(2\pi)^3}\mathrm{Tr}[\,\boldsymbol{\alpha}\mathcal{R}'\,] = 0, \tag{A.14}$$

which after some algebra results into

$$\frac{\partial\rho_\lambda}{\partial t} + \boldsymbol{\nabla}\cdot(\boldsymbol{v}\rho_\lambda) = 0, \tag{A.15}$$

in terms of the scaled baryon density ρ_λ. Once the scaling law of the baryon density with the λ parameter is specified, Eq. (A.15) will provide the connection between the velocity $\boldsymbol{v}$ and $\dot{\lambda}$.

Appendix B

The virial theorem results from homogeneity properties of the kinetic energy and potential energy components of the energy with respect to a scaling transformation that preserves the normalization [60]. For example, the scaling method has been employed to derive the virial theorem for the Skyrme interaction [19], or for relativistic particles bound in vector and scalar potentials [61]. Concerning the relativistic model discussed in the present work, we have given the expression of the first derivative of the scaled energy with respect to the scaling parameter λ in Eq. (3.8) of Section 3.2. It must vanish at $\lambda = 1$ (virial theorem):

$$0 = \left[\frac{\partial}{\partial \lambda} \int d(\lambda \boldsymbol{r}) \frac{\mathcal{H}_\lambda(\boldsymbol{r})}{\lambda^3} \right]_{\lambda=1}. \tag{B.1}$$

To evaluate the above equation knowledge of the derivatives of the scaled fields with respect to λ is required. Starting with the omega field V_λ, it fulfils the Klein–Gordon equation

$$(\Delta - m_{\rm v}^2) V_\lambda(\boldsymbol{r}) = -g_{\rm v} \rho_\lambda(\boldsymbol{r}), \tag{B.2}$$

whose solution is

$$V_\lambda(\boldsymbol{r}) = \frac{g_{\rm v}}{4\pi} \int d\boldsymbol{r}' \rho_\lambda(\boldsymbol{r}') \frac{e^{-m_{\rm v}|\boldsymbol{r}-\boldsymbol{r}'|}}{|\boldsymbol{r}-\boldsymbol{r}'|} = \int d(\lambda \boldsymbol{r}') \rho(\lambda \boldsymbol{r}') \mathcal{V}_\omega(s). \tag{B.3}$$

We employ the notation $\mathcal{V}_\omega(s) = g_{\rm v} \exp(-m_{\rm v} s)/4\pi s$, with $s = |\boldsymbol{r} - \boldsymbol{r}'|$, as in the main text. On defining $\boldsymbol{u} = \lambda \boldsymbol{r}$ and $\boldsymbol{u}' = \lambda \boldsymbol{r}'$ one obtains $V_\lambda(\boldsymbol{r}) = \int d\boldsymbol{u}' \rho(\boldsymbol{u}') \mathcal{V}_\omega(|\boldsymbol{u} - \boldsymbol{u}'|/\lambda)$, whence

$$\left. \frac{\partial V_\lambda(\boldsymbol{r})}{\partial \lambda} \right|_{\lambda=1} = -\int d\boldsymbol{r}' \rho(\boldsymbol{r}')\, s \frac{d\mathcal{V}_\omega(s)}{ds}, \tag{B.4}$$

in agreement with the result given in Ref. [57]. Analogous results are found for the scaled rho and Coulomb fields. The result for the scalar field is more complicated because an additional term appears due to the fact that the density $\tilde{\rho}_{\rm s}^{\rm eff}$ itself is a function of λ:

$$\left. \frac{\partial \phi_\lambda(\boldsymbol{r})}{\partial \lambda} \right|_{\lambda=1} = -\int d\boldsymbol{r}' \rho_{\rm s}^{\rm eff}(\boldsymbol{r}') s \frac{d\mathcal{V}_\sigma(s)}{ds} + \int d\boldsymbol{r}' \mathcal{V}_\sigma(s) \left[\frac{\partial \tilde{\rho}_{\rm s}^{\rm eff}(\lambda \boldsymbol{r}')}{\partial \lambda} \right]_{\lambda=1}. \tag{B.5}$$

Since $g_{\rm s} \tilde{\rho}_{\rm s}^{\rm eff} = g_{\rm s} \tilde{\rho}_{\rm s} - b\phi_\lambda^2/\lambda^3 - c\phi_\lambda^3/\lambda^3$, we have

$$g_{\rm s} \left. \frac{\partial \tilde{\rho}_{\rm s}^{\rm eff}}{\partial \lambda} \right|_{\lambda=1} = g_{\rm s} \left. \frac{\partial \tilde{\rho}_{\rm s}}{\partial \lambda} \right|_{\lambda=1} + 3(b\phi^2 + c\phi^3) - (2b\phi + 3c\phi^2) \left. \frac{\partial \phi_\lambda}{\partial \lambda} \right|_{\lambda=1}, \tag{B.6}$$

with

$$\left.\frac{\partial\tilde{\rho}_{\rm s}}{\partial\lambda}\right|_{\lambda=1} = \left.\frac{\delta\tilde{\rho}_{\rm s}}{\delta\tilde{m}^*}\frac{\partial\tilde{m}^*}{\partial\lambda}\right|_{\lambda=1} = -\frac{\delta\rho_{\rm s}}{\delta m^*}\left[m^* + g_{\rm s}\frac{\partial\phi_\lambda}{\partial\lambda}\right]_{\lambda=1}, \tag{B.7}$$

cf. Eq. (3.9) for $\partial\tilde{m}^*/\partial\lambda$.

From substitution into Eq. (B.1) of the derivatives (B.4) and (B.5) and of the corresponding results for the rho and Coulomb fields, on account of Eq. (3.8), one obtains

$$\begin{aligned} 0 &= \int d\boldsymbol{r}\left[\mathcal{E} - m^*\rho_{\rm s} + \frac{1}{2}g_{\rm s}\rho_{\rm s}^{\rm eff}\int d\boldsymbol{r}'\rho_{\rm s}^{\rm eff}(\boldsymbol{r}')s\frac{d\mathcal{V}_\sigma}{ds} - b\phi^3 - \frac{3}{4}c\phi^4\right. \\ &\quad \left. - \frac{1}{2}g_{\rm v}\rho\int d\boldsymbol{r}'\rho(\boldsymbol{r}')s\frac{d\mathcal{V}_\omega}{ds} - \frac{1}{2}g_\rho\rho_3\int d\boldsymbol{r}'\rho_3(\boldsymbol{r}')s\frac{d\mathcal{V}_\rho}{ds} + \frac{1}{2}e\mathcal{A}\rho_{\rm p}\right]. \end{aligned} \tag{B.8}$$

Now, using for example the relation $s\,d\mathcal{V}_\omega/ds = -\mathcal{V}_\omega - m_{\rm v}s\mathcal{V}_\omega$, it can be verified that

$$-\frac{1}{2}\int d\boldsymbol{r}g_{\rm v}\rho\int d\boldsymbol{r}'\rho(\boldsymbol{r}')s\frac{d\mathcal{V}_\omega}{ds} = \int d\boldsymbol{r}\left[\frac{1}{2}g_{\rm v}\rho V + m_{\rm v}^2V^2\right]. \tag{B.9}$$

After similar straightforward manipulations with the other fields, the virial theorem for the non-linear $\sigma-\omega$ model finally becomes

$$\begin{aligned} 0 &= \int d\boldsymbol{r}\left[\mathcal{E} - m^*\rho_{\rm s} - \frac{1}{2}g_{\rm s}\phi\rho_{\rm s} - m_{\rm s}^2\phi^2 - \frac{1}{2}b\phi^3 - \frac{1}{4}c\phi^4\right. \\ &\quad \left. + \frac{1}{2}g_{\rm v}V\rho + m_{\rm v}^2V^2 + \frac{1}{2}g_\rho R\rho_3 + m_\rho^2R^2 + \frac{1}{2}e\mathcal{A}\rho_{\rm p}\right]. \end{aligned} \tag{B.10}$$

One may notice that the quantity $\mathcal{E} - m^*\rho_{\rm s}$ corresponds to the semiclassical average of $\sum_i \varphi_i^\dagger\boldsymbol{\alpha}\cdot\boldsymbol{\nabla}\varphi_i$. Actually, in terms of the kinetic energy density τ (namely, the semiclassical counterpart of $\sum_i\varphi_i^\dagger[\boldsymbol{\alpha}\cdot\boldsymbol{\nabla} + \beta m - m]\varphi_i$) we can write $\mathcal{E} - m^*\rho_{\rm s} = \tau + m\rho - m\rho_{\rm s}$, which makes more obvious the kinetic energy component in the virial theorem. In the limit of symmetric infinite nuclear matter Eq. (B.10) goes over

$$\mathcal{E}_{0,\infty} - m^*_\infty\rho_{{\rm s},\infty} - \frac{3}{2}\frac{g_{\rm s}^2}{m_{\rm s}^2}{\rho_{{\rm s},\infty}^{\rm eff}}^2 - b\phi_\infty^3 - \frac{3}{4}c\phi_\infty^4 + \frac{3}{2}\frac{g_{\rm v}^2}{m_{\rm v}^2}\rho_\infty^2 = 3P = 0, \tag{B.11}$$

with P being the pressure, if equilibrium quantities are used.

Taking advantage of Eq. (B.10) to eliminate $\int d\boldsymbol{r}\mathcal{E}$ from the expression of $\int d\boldsymbol{r}\mathcal{H}$, the energy of a nucleus in the RMF model takes the remarkably simple form

$$\int d\boldsymbol{r}[\mathcal{H} - m\rho] = \int d\boldsymbol{r}\left[m(\rho_{\rm s} - \rho) + m_{\rm s}^2\phi^2 + \frac{1}{3}b\phi^3 - m_{\rm v}^2V^2 - m_\rho^2R^2\right], \tag{B.12}$$

where we have subtracted the nucleon rest mass contribution. This expression displays very clearly the relativistic mechanism for nuclear binding. It stems from the cancellation between the scalar and vector potentials and from the difference between the scalar density and the baryon density (i.e., from the small components of the wave functions). We have verified that Eqs. (B.10) and (B.12) are satisfied not only by the Thomas–Fermi solutions, but also by the ground-state densities and meson fields obtained from a quantal Hartree calculation. Of course, the energy stationarity condition of the RMF model against dilation must be fulfilled by any approximation scheme utilized to solve the problem.

References

[1] B.D. Serot and J.D. Walecka, Adv. Nucl. Phys. **16** (1986) 1; Int. J. of Mod. Phys. **E6** (1997) 515.

[2] J.D. Walecka, Ann. Phys. (N.Y.) **83**, 491 (1974).

[3] J. Boguta and A.R. Bodmer, Nucl. Phys. **A292** (1977) 413.

[4] G.A. Lalazissis, J. Köning and P. Ring, Phys. Rev. **C55** (1997) 540.

[5] G.F. Bertsch and S.F. Tsai, Phys. Rep. **18** (1975) 125.

[6] P. Ring and P. Schuck, The Nuclear Many-Body Problem, Springer-Verlag, Berlin, 1980.

[7] M. L'Huillier and Nguyen Van Giai, Phys. Rev. **C39** (1989) 2022; Zhong-yu Ma, Nguyen Van Giai, H. Toki and M. L'Huillier, Phys. Rev. **C55** (1997) 2385.

[8] J.F. Dawson and R.J. Furnstahl, Phys. Rev. **C42** (1990) 2009; C.J. Horowitz and J. Piekarewicz, Nucl. Phys. **A511** (1990) 461.

[9] J. Piekarewicz, Phys. Rev. **C64** (2001) 024307.

[10] D. Vretenar, H. Berghammer and P. Ring, Nucl. Phys. **A581** (1995) 679.

[11] D. Vretenar, G.A. Lalazissis, R. Behnsch, W. Pöschl and P. Ring, Nucl. Phys. **A621** (1997) 853.

[12] T. Maruyama and T. Suzuki, Phys. Lett. **B219** (1989) 43.

[13] H.F. Boersma, R. Malfliet and O. Scholten, Phys. Lett. **B269** (1991) 1.

[14] M.V. Stoitsov, P. Ring and M.M. Sharma, Phys. Rev. **C50** (1994) 1445.

[15] M.V. Stoitsov, M.L. Cescato, P. Ring and M.M. Sharma, J. Phys. **G20** (1994) L149.

[16] D. Von-Eiff, J.M. Pearson, W. Stocker and M.K. Weigel, Phys. Rev. **C50** (1994) 831.

[17] T. v. Chossy and W Stocker Phys. Rev. **C56** (1997) 2518.

[18] J.P. Blaizot, Phys. Rep. **64** (1980) 171.

[19] O. Bohigas, A.M. Lane and J. Martorell, Phys. Rep. **51** (1979) 267.

[20] Zhong-yu Ma, Nguyen Van Giai, A. Wandelt, D. Vretenar and P. Ring, Nucl. Phys. **A686** (2001) 173; P. Ring, Zhong-yu Ma, Nguyen Van Giai, D. Vretenar, A. Wandelt and Li-gang Cao, Nucl. Phys. **A694** (2001) 249.

[21] R.M. Dreizler and J. da Providência (Eds.), Density Functional Methods in Physics, Vol. 123 NATO ASI Series B, Plenum, New York, 1985; E.K.U. Gross and R.M. Dreizler (Eds.), Density Functional Theory, Vol. 337 NATO ASI Series B, Plenum, New York, 1995.

[22] M. Brack and R.K. Bhaduri, Semiclassical Physics, Addison-Wesley, Reading, 1997.

[23] I.Zh. Petkov and M.V. Stoitsov, Nuclear Density Functional Theory, Clarendon Press, Oxford, 1991.

[24] G. Eckart, G. Holzwarth and J.P. da Providência, Nucl. Phys. **A364** (1981) 1.

[25] M. Brack, C. Guet and H.-B. Håkansson, Phys. Rep. **123** (1985) 275.

[26] M. Centelles, M. Pi, X. Viñas, F. Garcias and M. Barranco, Nucl. Phys. **A510** (1990) 397.

[27] P. Gleissl, M. Brack, J. Meyer and P. Quentin, Ann. Phys. (N.Y.) **197** (1990) 205.

[28] J.D. Walecka, Phys. Lett. **94B** (1980) 293; C.J. Horowitz and J.D. Walecka, Nucl. Phys. **A364** (1981) 429.

[29] R.J. Furnstahl and B.D. Serot, Acta Physica Polonica **B16** (1985) 875.

[30] C. da Providência, L. Brito, J. da Providência, M. Nielsen and X. Viñas, Phys. Rev. **C54** (1996) 2525.

[31] S. Nishizaki, H. Kurasawa and T. Suzuki, Nucl. Phys. **A462** (1987) 689.

[32] Chaoyuan Zhu and Xi-Jun Qiu, J. Phys. **G17** (1991) L11.

[33] M. Centelles, X. Viñas, M. Barranco and P. Schuck, Nucl. Phys. **A519** (1990) 73c.

[34] M. Centelles, X. Viñas, M. Barranco and P. Schuck, Ann. of Phys. (N.Y.) **221** (1993) 165.

[35] C. Speicher, R.M. Dreizler and E. Engel, Ann of Phys. (N.Y.) **213** (1992) 312.

[36] M. Centelles, X. Viñas, M. Barranco, S. Marcos and R.J. Lombard, Nucl. Phys. **A537** (1992) 486.

[37] C. Speicher, E. Engel and R.M. Dreizler, Nucl. Phys. **A562** (1993) 569.

[38] M. Centelles and X. Viñas, Nucl. Phys. **A563** (1993) 173.

[39] M. Centelles, M. Del Estal and X. Viñas, Nucl. Phys. **A635** (1998) 193.

[40] S.K. Patra, M. Centelles, X. Viñas and M. Del Estal, Phys. Lett. **B** (2001), in press.

[41] F.E. Bertrand, Ann. Rev. Nucl. Part. Sci. **26** (1976) 457; J. Speth and A. Van der Woude, Rep. Prog. Phys. **44** (1981) 719; K. Goeke and J. Speth, Ann. Rev. Nucl. Part. Sci. **32** (1982) 65.

[42] D.H. Youngblood, H.L. Clark and Y.-W. Lui, Phys. Rev. Lett. **82** (1999) 691; D.H. Youngblood, Y.-W. Lui and H.L. Clark, Phys. Rev. **C63** (2001) 067301.

[43] P.-G. Reinhard, M. Rufa, J. Maruhn, W. Greiner and J. Friedrich, Z. Phys. **A323** (1986) 13.

[44] M.M. Sharma, M.A. Nagarajan and P. Ring, Phys. Lett. **B312** (1993) 377.

[45] S.J. Lee, J. Fink, A.B. Balantekin, M.R. Strayer, A.S. Umar, P.-G. Reinhard, J.A. Maruhn and W. Greiner, Phys. Rev. Lett. **57** (1986) 2916; *ibid* **59** (1987) 1171.

[46] S.K. Patra, R.K. Gupta and W. Greiner, Int. J. Mod. Phys. **E6** (1997) 641; S.K. Patra, C.-L. Wu, C.R. Praharaj and R.K. Gupta, Nucl. Phys. **A651** (1999) 117.

[47] J.P. Blaizot, J.F. Berger, J. Dechargé and M. Girod, Nucl. Phys. **A591** (1995) 435.

[48] M. Farine, J.M. Pearson and F. Tondeur, Nucl. Phys. **A615** (1997) 135.

[49] S. Shlomo and D.H. Youngblood, Phys. Rev. **C47** (1993) 529.

[50] P.-G. Reinhard, Rep. Prog. Phys. **52** (1989) 439.

[51] R.J. Furnstahl, C.E. Price and G.E. Walker, Phys. Rev. **C36** (1987) 2590.

[52] M. Rashdan, Phys. Rev. **C63** (2001) 044303.

[53] J.P. Blaizot, D. Gogny and B. Grammaticos, Nucl. Phys. **A265** (1976) 315; J.P. Blaizot and B. Grammaticos, Nucl. Phys. **A355** (1981) 115.

[54] J. Treiner, H. Krivine, O. Bohigas and J. Martorell, Nucl. Phys. **A371** (1981) 253.

[55] S.K. Patra, M. Centelles, X. Viñas and M. Del Estal, submitted to Phys. Rev. **C** (2001).

[56] I. Hamamoto, H. Sagawa and X.Z. Zhang, Phys. Rev. **C56** (1997) 3121.

[57] M. Kohno and K. Ando, Prog. Theor. Phys. **61** (1979) 1065.

[58] B.K. Jennings, Phys. Lett. **B96** (1980) 1.

[59] G. Baym and S.A. Chin, Nucl. Phys. **A262** (1976) 527.

[60] For scaling relations and the virial theorem see, e.g., R.G. Parr and W. Yang, Density-Functional Theory of Atoms and Molecules (Oxford University Press, New York, 1989), and references therein.

[61] M. Brack, Phys. Rev. **D27** (1983) 1950.

Figure captions

Figure 1. The breathing-mode energies from the RETF scaling calculations are compared with the empirical law $80/A^{1/3}$ MeV and the experimental data reported in Ref. [49], as a function of the size of the nucleus.

Figure 2. Scaling incompressibility of some finite nuclei as obtained in the RETF calculations versus the nuclear matter incompressibility for various relativistic parameter sets. The value of K_∞ of each set is listed in MeV. The straight lines are linear fits. The fit for ^{208}Pb is drawn by a solid line.

Figure 3. Monopole excitation energy from RETF scaling calculations versus the nuclear matter incompressibility for various relativistic parameter sets. The value of K_∞ of each set is given in Figure 2. The dashed lines are linear fits to the square root of K_∞.

Figure 4. Monopole excitation energy of ^{208}Pb from RETF scaling calculations, as a function of the mass of the scalar meson and of the nuclear matter effective mass of the relativistic interaction. The dashed lines show the sense of increasing K_∞.

Table 1: Excitation energy of the monopole state (in MeV) obtained in the scaling approach by using various relativistic parameter sets (in order of increasing value of the compression modulus K_∞). The experimental centroid energies are from Ref. [42].

	NL1		NL3		NL-SH		NL2			
	RTF	RETF	RTF	RETF	RTF	RETF	RTF	RETF	$80A^{-1/3}$	Exp.
^{16}O	25.1	23.3	27.5	27.8	30.7	33.1	34.4	35.6	31.7	
^{40}Ca	21.2	20.6	23.5	24.1	26.6	28.2	29.5	30.3	23.4	19.2 ± 0.4
^{48}Ca	20.0	19.5	22.3	22.7	25.2	26.5	27.7	28.3	22.0	
^{90}Zr	17.2	16.9	19.2	19.5	21.9	22.8	24.0	24.5	17.9	17.9 ± 0.2
^{116}Sn	15.9	15.6	17.7	18.0	20.3	21.0	22.3	22.6	16.4	16.1 ± 0.1
^{144}Sm	14.9	14.6	16.6	16.8	19.0	19.6	20.8	21.1	15.3	15.4 ± 0.3
^{208}Pb	12.9	12.7	14.5	14.6	16.6	17.0	18.1	18.4	13.5	14.2 ± 0.3

Table 2: Comparison of the giant monopole resonance energies (in MeV) obtained in the scaling model with those obtained in the relativistic RPA [9].

	NLC			NLB			L2′		
	RTF	RETF	RRPA	RTF	RETF	RRPA	RTF	RETF	RRPA
^{40}Ca	22.5	22.4	21.0	27.7	29.4	27.9	29.1	33.0	27.3
^{90}Zr	18.1	18.1	16.9	23.3	24.2	24.1	25.2	27.4	26.5
^{208}Pb	13.6	13.5	13.1	18.0	18.5	18.1	19.9	21.0	20.1

Table 3: Monopole excitation energy (in MeV) obtained by constrained calculations with various parameter sets. The constrained RMF results are from Ref. [14] and the generator coordinate method results are from Ref. [11].

	NL1			NL3		NL-SH			NL2	
	RETF	CRMF	GCM	RETF	GCM	RETF	CRMF	GCM	RETF	GCM
^{16}O	21.8	20.9	20.2	26.0	22.6	30.0	25.8	25.0	32.4	27.1
^{40}Ca	19.8	19.2	16.6	23.2	19.6	26.9	23.9	22.0	29.0	24.4
^{90}Zr	16.5	16.3	14.1	19.1	16.9	22.1	21.1	19.5	23.7	21.9
^{208}Pb	12.1	12.2	11.0	14.0	13.0	16.2	16.1	15.0	17.4	16.6

Table 4: Excitation energy of the quadrupole vibration (in MeV) obtained in the scaling approach. The experimental values are from Ref. [41].

	NL1	NL3	NL-SH	NL2	LZ	$65A^{-1/3}$	Exp.
^{16}O	21.6	22.9	24.0	24.7	25.8	25.8	22.0
^{40}Ca	17.9	18.6	19.2	19.4	20.8	19.0	18.0
^{48}Ca	16.9	17.5	18.1	18.1	19.5	17.9	
^{90}Zr	14.4	14.8	15.2	15.1	16.4	14.5	14.5
^{208}Pb	10.9	11.2	11.5	11.3	12.4	11.0	10.5

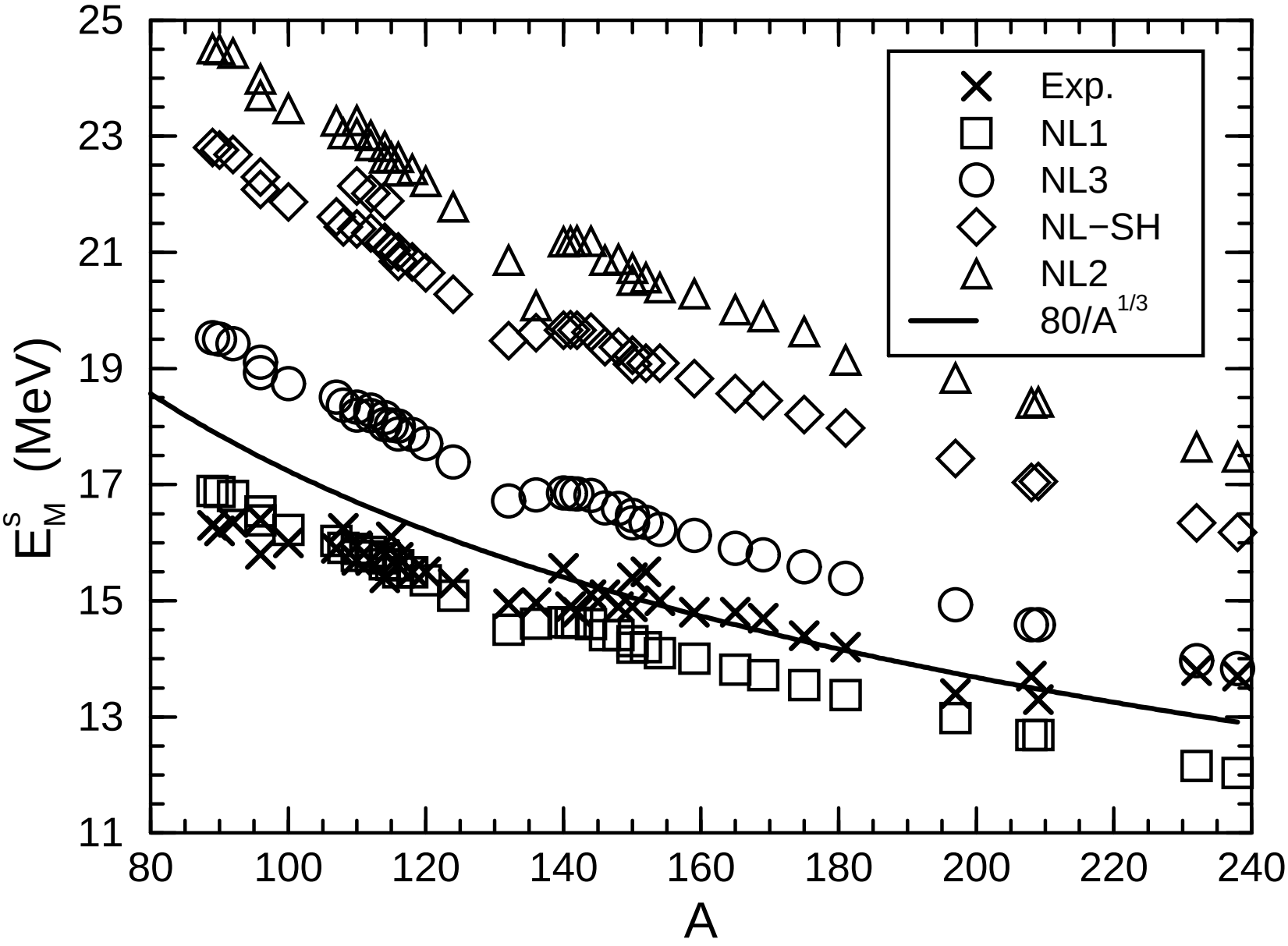
25
23
21
19
17
15
13
11
80
100
120
140
160
180
200
220
240
A
E_M^s (MeV)
Exp.
NL1
NL3
NL−SH
NL2
$80/A^{1/3}$

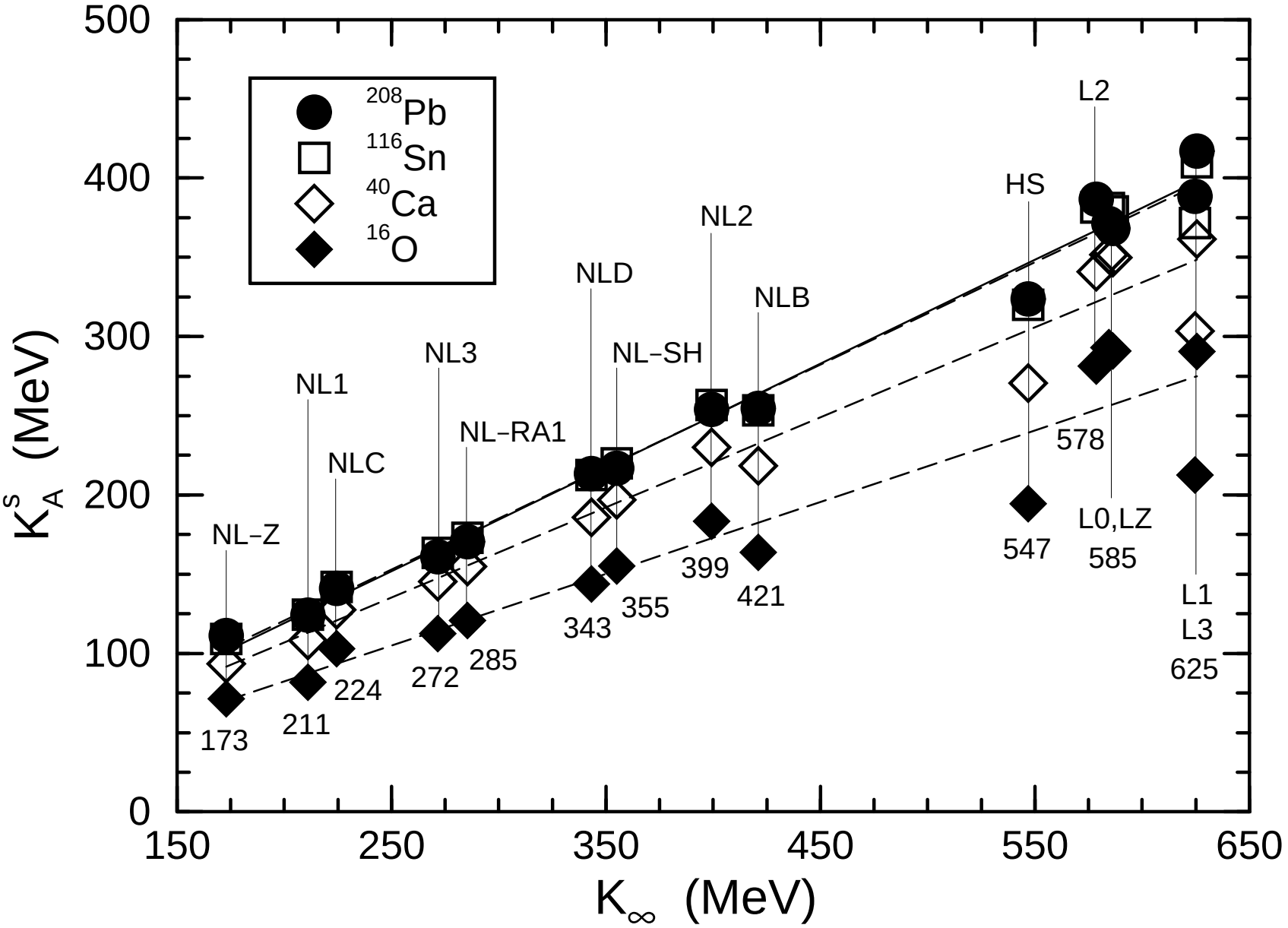
^{208}Pb
^{116}Sn
^{40}Ca
^{16}O
NL−Z
NL1
NLC
NL3
NL−RA1
NLD
NL−SH
NL2
NLB
HS
L2
L0,LZ
L1
L3
173
211
224
272
285
343
355
399
421
547
578
585
625
K_A^s (MeV)
K_∞ (MeV)
0
100
200
300
400
500
150
250
350
450
550
650

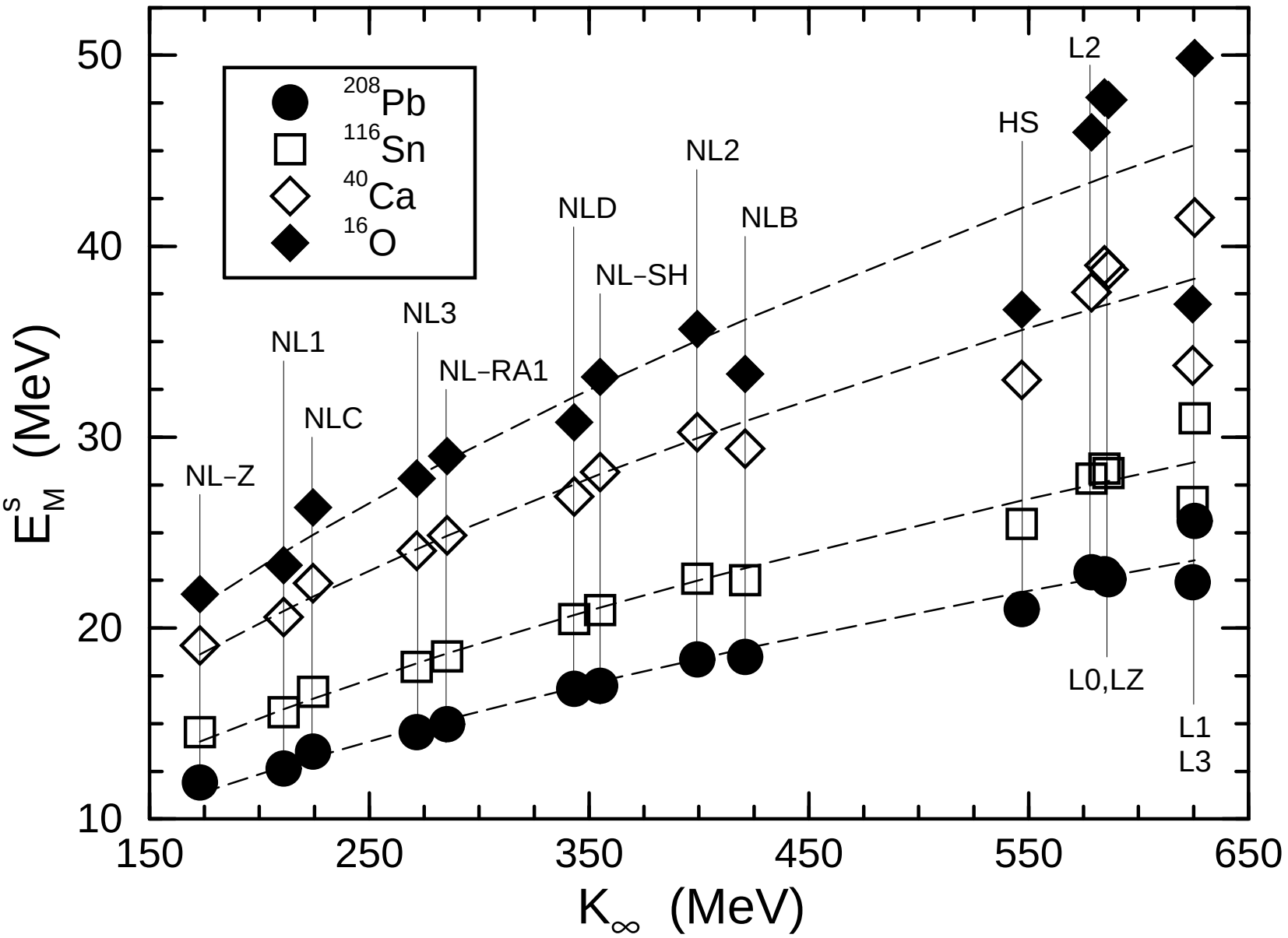
^{208}Pb
^{116}Sn
^{40}Ca
^{16}O
NL−Z
NL1
NLC
NL3
NL−RA1
NLD
NL−SH
NL2
NLB
HS
L2
L0,LZ
L1
L3
E_M^s (MeV)
K_∞ (MeV)
10
20
30
40
50
150
250
350
450
550
650

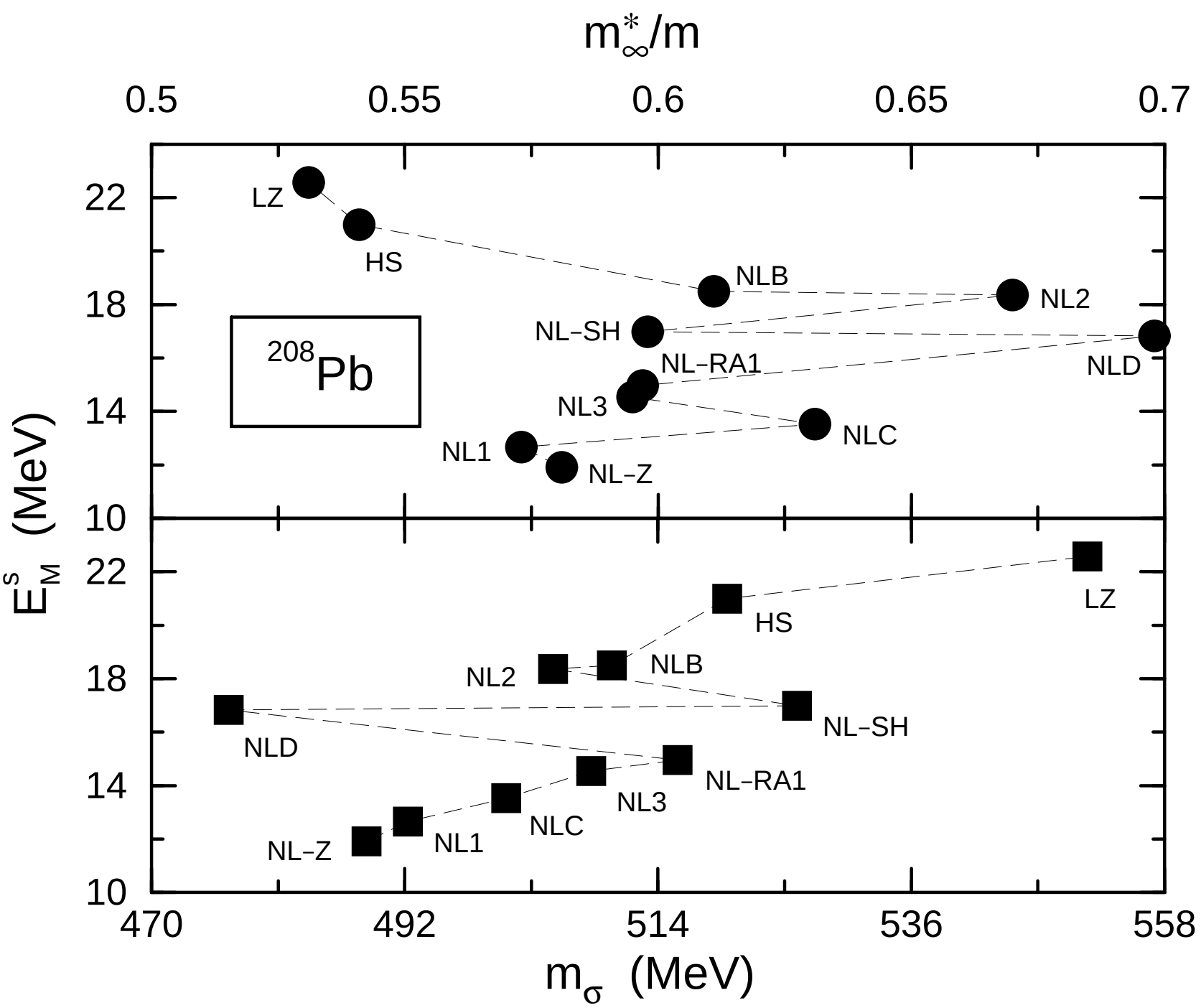
m^*_∞/m
0.5
0.55
0.6
0.65
0.7
^{208}Pb
LZ
HS
NLB
NL2
NL–SH
NL–RA1
NLD
NL3
NLC
NL1
NL–Z
E^s_M (MeV)
22
18
14
10
m_σ (MeV)
470
492
514
536
558